Available online at www.sciencedirect.com

ScienceDirect

Geochimica et Cosmochimica Acta 292 (2021) 364–381

Geochimica et Cosmochimica Acta

www.elsevier.com/locate/gca

Sr-Nd-Hf-O isotope constraints on crustal contamination and mantle source variation of three Fe-Ti-V oxide ore deposits in the Emeishan large igneous province

Qingyan Tang [a], Chusi Li [b,c,*], Edward M. Ripley [c], Jian Bao [a], Tianbao Su [a], Shihai Xu [a]

[a] School of Earth Sciences and Key Laboratory of Mineral Resources in Western China (Gansu Province), Lanzhou University, Lanzhou 730000, China

[b] State Key Laboratory of Ore Deposit Geochemistry, Institute of Geochemistry, Chinese Academy of Sciences, Guiyang 550002, China

[c] Department of Geological and Atmospheric Sciences, Indiana University, Bloomington, IN 47405, USA

Received 24 April 2020; accepted in revised form 5 October 2020; available online 13 October 2020

Abstract

Magma-carbonate interaction and recycled oceanic crust in the mantle source are thought to have played a critical role in the genesis of magmatic Fe-Ti-V oxide ore deposits in the Emeishan mantle plume-related large igneous province in southwestern China. To test these hypotheses, we have carried out a combined study of zircon Hf-O isotopes and whole-rock Sr-Nd isotopes on three representative magmatic Fe-Ti-V oxide ore deposits associated with different types of wall-rock in the province: the Hongge and Taihe deposits with granitoid wall-rocks in most places, and the Panzhihua deposit with marble wall-rocks. Diopside-garnet marble xenoliths are common in the host gabbros of the Taihe deposit. The zircon separates used in this study are all from the mineralized units of the host layered mafic–ultramafic intrusions. The selected zircon grains yield U-Pb isotopic ages of 258.2 ± 2.8 Ma for Hongge intrusion, 263.3 ± 2.2 Ma for Taihe intrusion, and 257.6 ± 2.1 Ma for Panzhihua intrusion. The Hf-O isotopes of the zircon separates are $\varepsilon_{Hf}(t)$ from 3.1 to 4.7 and $\delta^{18}O$ from 5.77 to 6.45‰ for Hongge, $\varepsilon_{Hf}(t)$ from 8.3 to 9.8 and $\delta^{18}O$ from 4.12 to 4.56‰ for Taihe, and $\varepsilon_{Hf}(t)$ from 4.6 to 6.3 and $\delta^{18}O$ from 5.49 to 6.10‰ for Panzhihua. The zircon $\delta^{18}O$ values of the Taihe deposit are significantly lower than the mantle zircon values (5.3 ± 0.3‰), whereas those of the Hongge and Panzhihua deposits are higher than the mantle values. The initial $^{87}Sr/^{86}Sr$ and $\varepsilon_{Nd}(t)$ of the whole rock samples from the deposits are similar, from 0.7047 to 0.7052 and from 2.3 to 3.1, respectively. The observed decoupling of zircon Hf-O isotopes (low $\delta^{18}O$ and high $\varepsilon_{Hf}(t)$ values) in the Taihe deposit is most consistent with a high-temperature altered, low $\delta^{18}O$ oceanic gabbroic component in the plume source for this deposit. All of the isotope data together show that the parental magmas for these deposits experienced different types of crustal contamination. Contamination with the Precambrian metamorphic country rocks is much more significant in the parental magma for the Hongge deposit than those for the Panzhihua and Taihe deposits. On the other hand, contamination with marble country rocks is more pronounced in the parental magmas for the Panzhihua and Taihe deposits than in the parental magma for the Hongge deposit.

* Corresponding author at: State Key Laboratory of Ore Deposit Geochemistry, Institute of Geochemistry, Chinese Academy of Sciences, Guiyang 550002, China.

E-mail address: cli@indiana.edu (C. Li).

https://doi.org/10.1016/j.gca.2020.10.006

An important new finding from this study is that these deposits are not linked to the same component of the mantle plume nor a single type of crustal contamination.

Keywords: Zircon U-Pb ages; Zircon Hf-O isotopes; Whole-rock Sr-Nd isotopes; Fe-Ti-V oxide ore deposits; Emeishan large igneous province

1. INTRODUCTION

The Permian Emeishan large igneous province (LIP), which occurs in SW China and northern Vietnam, contains several large magmatic Fe-Ti-V oxide ore deposits associated with relatively small layered mafic–ultramafic intrusions, such as the Panzhihua, Hongge, and Taihe intrusions (Fig. 1). These intrusions are much smaller than the Bushveld Complex in South Africa, a large layered mafic–ultramafic intrusion with significant Fe-Ti oxide mineralization in the upper part (Tegner et al., 2006). The magmatic Fe-Ti oxide ores in the Emeishan LIP are related to the emplacement and differentiation of high-Ti basalts in the crust (e.g., Zhou et al., 2005; Pang et al., 2008; Zhang et al., 2009; Hou et al., 2011, 2012; Bai et al., 2014). Some researchers have suggested that the parental magmas for these deposits are derivatives of mantle-derived magma produced by partial melting related to a rising Permian mantle plume that entrained ancient recycled, Fe-Ti rich oceanic crust (Zhang et al., 2009; Hou et al., 2011, 2012). Other researchers have attributed the assumed high Fe-Ti contents in the parental magmas to be the results of interaction between magma derived from mantle plume and a Late Paleozoic subducted oceanic lithospheric slab that occurred above the ascending plume-derived magma (Bai et al., 2014). A third model focusses on enrichment in Fe and Ti related to extensive fractional crystallization of olivine at depth from the mantle-derived Mg-rich magma (Song et al., 2013).

With respect to mineralization at Panzhihua, where the immediate wall rocks of the deposit are marbles, Ganino et al. (2008) suggested that interaction between magma and the marble wall-rocks played a critical role in the formation of this deposit. They proposed that the CO_2-rich fluids released from the marble wall-rocks during contact metamorphism could oxidize the magma, convert some Fe^{2+} to Fe^{3+} in the magma and thereby induce crystallization of abundant magnetite from the contaminated magma. Xing et al. (2012) claimed that the C-H-O isotope compositions of volatiles extracted from mineral separates of this deposit support the ore genetic model of Ganino et al. (2008), although the interpretation of the volatile isotope data by Xing et al. (2012) represents only one of several possibilities. Tang et al. (2017a) reported the mineralogy and Sr-Nd isotopes of samples from a small picritic dyke (<20 m across) extending from the marginal zone of the Panzhihua deposit into the marble country rock. Their data are consistent with up to 20 wt.% of marble assimilation in the outmost margin of the dyke that is characterized by an unusual association of magnetite with Mg-rich olivine (~90 Fo mol%). Such an unusual mineralogical association is also present in some of the oxide ore layers of the Panzhihua deposit, albeit the Fo contents of olivine in the ore layers are much lower (65–70 mol%, Bai et al., 2014). This precarious similarity, together with the inference of significant marble assimilation in the margin of the picritic dyke from Sr isotope data, has been used by some researchers (Tang et al., 2017a) as supporting evidence for the ore genetic model of Ganino et al. (2008). However, some questions still exist. Most importantly, more complete Sr-Nd-O isotope data for the Panzhihua deposit show no widespread significant contamination of magma by the carbonate country rock at Panzhihua, similar to the results for the other coeval magmatic Fe-Ti-V oxide ore deposits that are not surrounded by carbonates in the region, such as the Hongge and Taihe deposits (Yu et al., 2015). Based on these results, these authors ruled out carbonate assimilation as an important genetic process for these deposits.

To test the different genetic hypotheses described above, we have carried out a combined zircon Hf-O isotope study of the Panzhihua, Hongge and Taihe deposits. The zircon separates from these deposits have been dated using the U-Pb method, and the whole-rock samples used for zircon separation have been analyzed for Sr-Nd isotopes. Zircon was chosen for this study because the mineral has a high closure temperature and its Hf-O isotopes are generally not susceptible to post-magmatic alteration (Griffin et al., 2002; Valley, 2003; Belousova et al., 2006). The combination of Hf and O isotopes of dated zircon crystals has been successfully used to trace the mantle sources of magma and to distinguish different types of contamination (e.g., Griffin et al., 2002; Belousova et al., 2006; Zhang et al., 2016; Zhu et al., 2017). No similar study has been previously undertaken of the magmatic Fe-Ti-V oxide ore deposits in the Emeishan LIP. Previously, zircons from some of these deposits were analyzed for Lu-Hf isotopes but not for O isotopes (Zhong et al., 2011a; Shellnutt et al., 2011). In this study we focus on potential variations in mantle sources and the role of different types of contamination in ore genesis. We have selected the Panzhihua, Hongge and Taihe deposits for this study because these deposits are hosted by different types of country rocks and the Fo contents of olivine in these deposits cover the entire range for this type of deposit in the Emeishan LIP.

2. GEOLOGICAL BACKGROUND

2.1. Emeishan large igneous province

The Emeishan LIP is $\sim 2.5 \times 10^5$ km^2 extending from SW China to northern Vietnam (Fig. 1). It is composed of Permian flood basalts and associated mafic–ultramafic

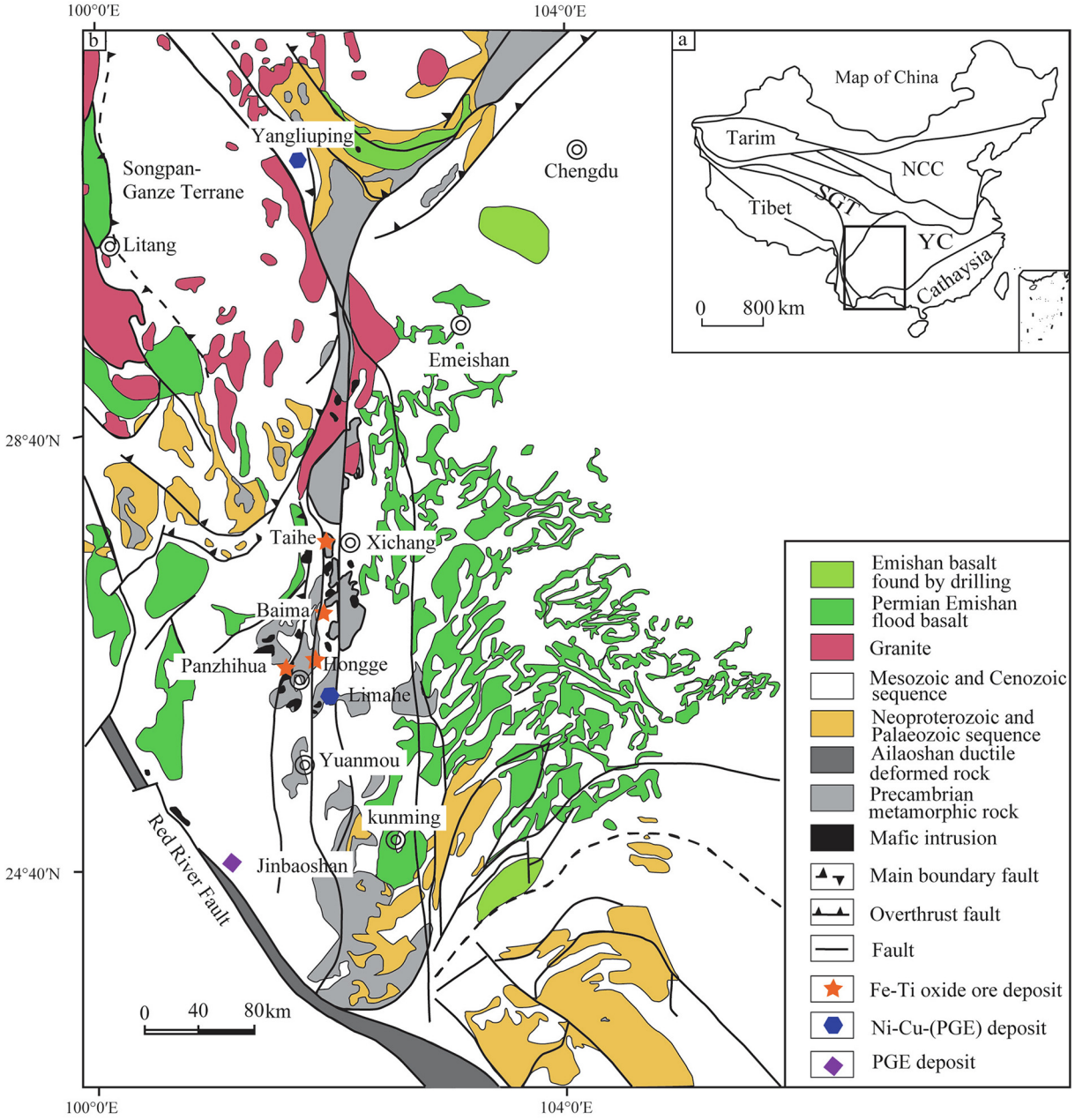

Fig. 1. Distribution of Permian flood basalts and coeval mafic–ultramafic intrusions in the Emeishan large igneous province (after Li et al., 2016, and references therein). NCC = North China Craton, SGT = Songpan-Ganzi terrane, YC = Yangtze Craton.

intrusions. Picrites, basalts and basaltic andesites are the major volcanic rocks (Chung and Jahn, 1995; Xu et al., 2001; Tang et al., 2015; Li et al., 2016). The basalts can be further divided into high-Ti and low-Ti series (Xu et al., 2001). The associated mafic–ultramafic intrusions are mostly exposed in the central part of the province as a result of severe post-Permian uplift and erosion in this region. The zircon U-Pb ages of these intrusions and coeval basalts in the Emeishan LIP vary from ~256 to ~263 Ma (e.g., Zhou et al., 2008; Fan et al., 2008; Zi et al., 2010; Zhong et al., 2011a; Tang et al., 2015). The low-Ti mafic–ultramafic intrusions and the high-Ti gabbroic intrusions in the Emeishan LIP host some important magmatic Cu-Ni-(PGE) sulfide and Fe-Ti-V oxide ore deposits, respectively (Fig. 1). The mafic–ultramafic intrusions with significant Ni-Cu-PGE sulfide mineralization are the Baimazhai, Limahe, Jinbaoshan and Zhubu intrusions (e.g., Tao et al., 2007, 2008; Song et al., 2008). Based on the concept that the coeval mafic–ultramafic intrusive and extrusive rocks of the same igneous event, such as mantle plume activity, could be genetically linked, Zhou et al. (2008) suggested that the parental magmas for the sulfide-mineralized and the oxide-mineralized intrusions are the equivalents of the low-Ti and high-Ti basalts, respectively.

2.2. Magmatic Fe-Ti-V oxide deposits

Many gabbroic intrusions in the Emeishan LIP contain significant Fe-Ti-V oxide mineralization. Several of them, such as Baima, Hongge, Panzhihua and Taihe, host giant Fe-Ti-V oxide ore deposits (Fig. 1). The total reserve of these four deposits together exceeds 10 billion metric tons (Mt) of ores with 25–35 wt.% Fe, 4–13 wt.% Ti and 0.1–0.45 wt.% V (Panxi Geological Unit, 1984). The TiO_2 and V_2O_5 reserves are 32,390 and 683 Mt for Hongge, 9709 and 208 Mt for Panzhihua, 6223 and 232 Mt for Taihe, and 4496 and 337 Mt for Baima (Wen et al., 2008). Compared to other important magmatic Fe-Ti oxide ore deposits that occur elsewhere in the world, the deposits in the Emeishan LIP are characterized by much smaller sizes of the host intrusions, the appearance of the mineralization in the lower parts instead of the upper parts of the host intrusions, and higher Fo contents of olivine in the ore zones (Zhou et al., 2008; Pang et al., 2009).

2.2.1. Panzhihua

The Panzhihua intrusion is predominantly composed of gabbros (Fig. 2a). The surface exposure of the Panzhihua intrusion is ~19 km in length, ~2 km in thickness with an outcrop area of ~30 km^2 (Zhou et al., 2005). It dips northwest at angles ranging from 40° to 60°. It was emplaced into Neoproterozoic dolomitic limestones. Contact metamorphism produced up to 300 m-thick forsterite and diopside marbles in the lower contact (Pang et al., 2008). Elsewhere the intrusion is in fault contact with late-Permian syenites and Triassic terrestrial clastic sedimentary rocks. The Panzhihua intrusion is further divided into the Marginal, Lower, Middle and Upper Zones (Fig. 2a). Abundant apatite is present in the Middle Zone. The most important Fe-Ti-V oxide ore layers occur in the Lower Zone (Pang et al., 2008; Yu et al., 2015; Cao et al., 2019).

2.2.2. Hongge

The Hongge intrusion crops out over an area of about 60 km^2 to the northeast of Panzhihua city (Fig. 1). It is ~15 km in length, 3–5 km in width, 1.2 km in thickness, dipping to the southeast with angles of 50–60° (Fig. 2b). This intrusion is in contact with Mesoproterozoic schists and meta-sandstones in the north, with Neoproterozoic dolomitic limestones in the south, and with the Permian flood basalts of the Emeishan LIP in the northeast (Bai et al., 2012a, 2012b; Panxi Geological Unit, 1984). The dolomitic limestone in contact with the intrusion has been metamorphosed to marble in places (Luan et al., 2014). The west and north contact zones of the intrusion were

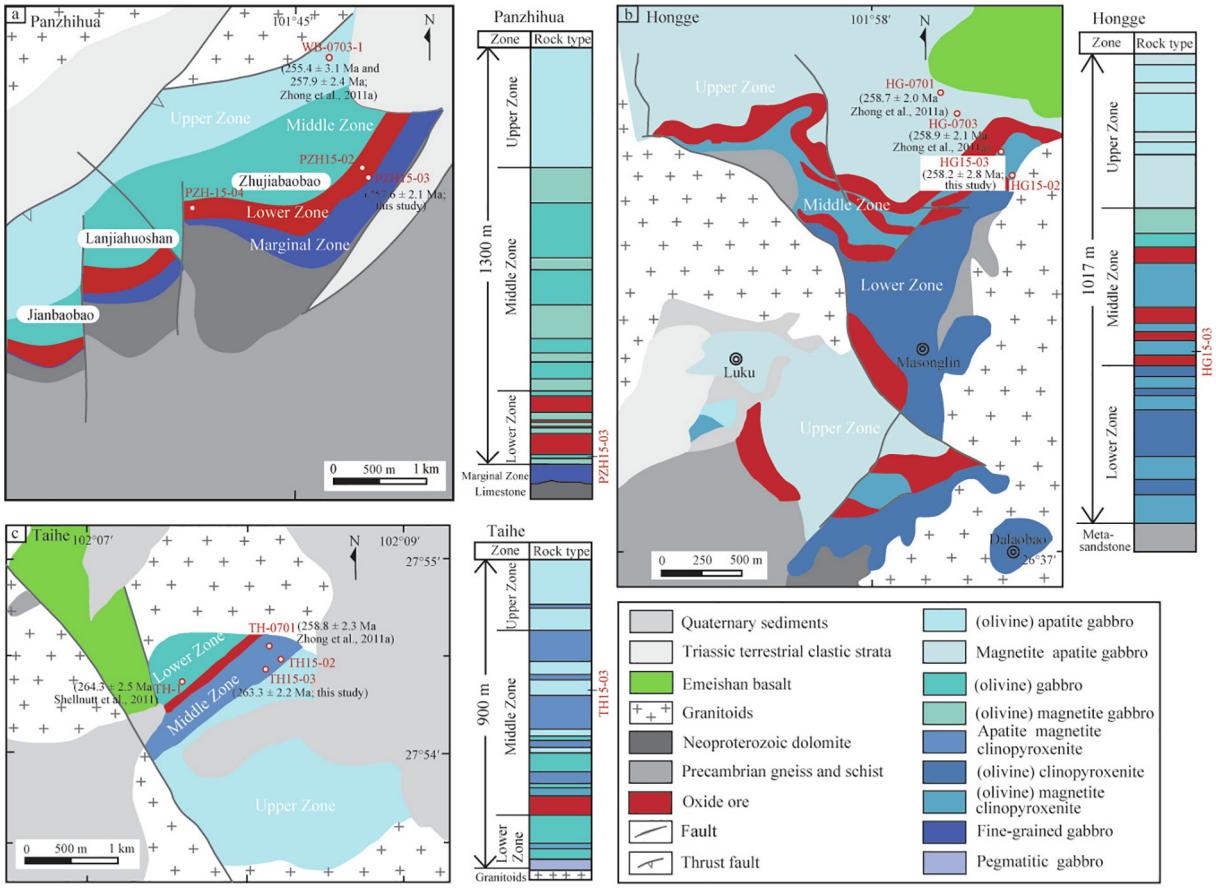

Fig. 2. Simplified plan views and lithological columns of the Panzhihua (a), Hongge (b) and Taihe (c) Fe-Ti-V oxide ore-bearing layered intrusions in the Emeishan large igneous province (modified from Song et al., 2013; Luan et al., 2014; She et al., 2014; Yu et al., 2015).

intruded by the late Permian alkaline granites and alkaline syenites (255.2 ± 3.6 Ma, Xu et al., 2008). The Hongge intrusion is divided into the Lower, Middle and Upper Zones (Fig. 2). The base of the Upper Zone is defined by the appearance of abundant euhedral apatite. The most important Fe-Ti-V oxide ore layers mainly occur in the upper part of the Lower Zone and the lower part of the Middle Zone (Zhong et al., 2002).

2.2.3. Taihe

The Taihe intrusion occurs in the central part of the Emeishan LIP (Fig. 1). It is ~3 km in length, ~2 km in width and ~1.2 km in thickness, dipping to southeast with angles of 50–60° (Fig. 2c). Diopside-garnet marble xenoliths are common in the Taihe intrusion (Panxi Geological Unit, 1984). The immediate country rocks of the intrusion are Permian syenites (261 ± 2 Ma, Xu et al., 2008). The Taihe intrusion is divided into Lower, Middle and Upper Zones (Fig. 2c). Abundant apatite occurs in the Middle Zone and Upper Zone. Important Fe-Ti-V oxide mineralization occurs as concordant semi-massive oxide layers throughout the intrusion as well as a thick massive oxide layer in the lower part of the Middle Zone (Panxi Geological Unit, 1984).

3. SAMPLES AND ANALYTICAL METHODS

3.1. Samples

Zircon crystals for O-Hf isotope analyses were separated from a large sample (5–10 kg) from each of the three selected intrusions in the Emeishan LIP: a gabbro sample (PZH15-03) from the Panzhihua intrusion, a clinopyroxenite sample (HG15-03) from the Hongge intrusion, and a gabbro sample (TH15-03) from the Taihe intrusion. These samples, and those collected for whole-rock Sr-Nd isotope analyses, are shown in the plan views of the intrusions (Fig. 2a–c). Each of these intrusions are divided into three

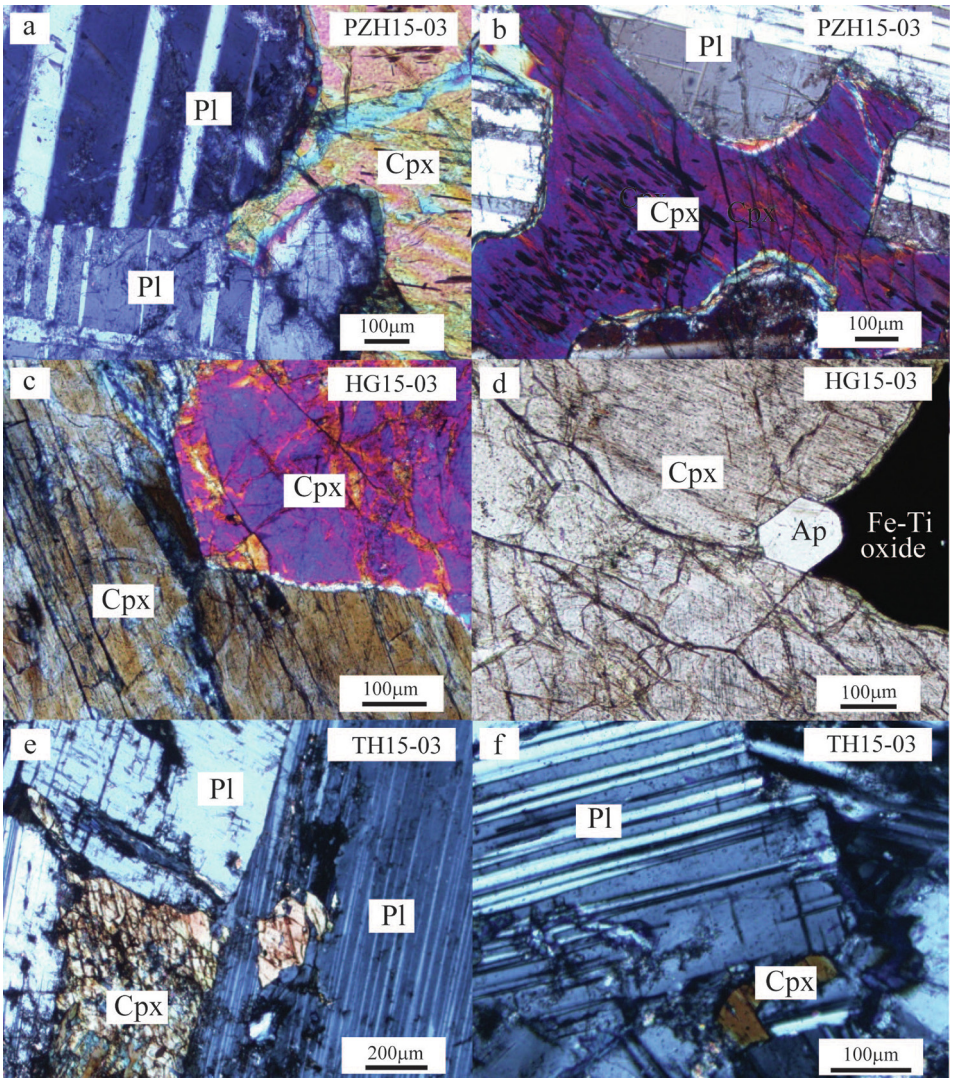

Fig. 3. Photomicrographs of samples for zircon separates from the Panzhihua (a, b), Hongge (c, d) and Taihe (e, f) intrusions. *Cpx*, clinopyroxene; *Pl*, plagioclase; *Ap*, apatite.

Table 1
SIMS zircon U-Pb isotope data for the Hongge, Panzhihua and Taihe Fe-Ti-V oxide ore-bearing mafic–ultramafic intrusions.

Sample/spot	U (ppm)	Th (ppm)	Th/U	f_{206} (%)	$^{207}Pb/^{206}Pb$	1σ (%)	$^{207}Pb/^{235}U$	1σ (%)	$^{206}Pb/^{238}U$	1σ (%)	$^{207}Pb/^{235}U$ age (Ma)	1σ	$^{206}Pb/^{238}U$ age (Ma)	1σ
Zircon from the Panzhihua gabbro (N26°37.849′, E101°45.227′, H 1164 m)														
PZH15-03-1	548	527	0.961	0.15	0.05141	1.39	0.28802	2.14	0.0406	1.63	257.0	4.9	256.7	4.1
PZH15-03-2	148	119	0.808	0.68	0.05217	2.04	0.29320	2.60	0.0408	1.61	261.1	6.0	257.5	4.1
PZH15-03-3	687	901	1.313	0.15	0.05167	1.04	0.28965	1.83	0.0407	1.51	258.3	4.2	256.9	3.8
PZH15-03-4	209	196	0.937	0.21	0.05173	1.73	0.28952	2.31	0.0406	1.53	258.2	5.3	256.5	3.8
PZH15-03-5	151	82	0.546	0.41	0.05189	2.80	0.28770	3.29	0.0402	1.73	256.7	7.5	254.2	4.3
PZH15-03-6	177	101	0.570	0.45	0.05074	1.92	0.28118	2.48	0.0402	1.58	251.6	5.5	254.0	3.9
PZH15-03-7	116	78	0.672	0.90	0.05144	2.41	0.29092	2.87	0.0410	1.56	259.3	6.6	259.1	4.0
PZH15-03-8	304	128	0.422	0.31	0.05152	1.43	0.29196	2.09	0.0411	1.53	260.1	4.8	259.7	3.9
PZH15-03-9	337	347	1.029	0.21	0.05158	1.38	0.28794	2.04	0.0405	1.50	256.9	4.6	255.9	3.8
PZH15-03-10	361	349	0.967	0.20	0.05162	2.15	0.28760	2.75	0.0404	1.71	256.7	6.2	255.3	4.3
PZH15-03-11	316	297	0.941	0.37	0.05215	1.41	0.29309	2.16	0.0408	1.64	261.0	5.0	257.5	4.1
PZH15-03-12	130	74	0.565	0.67	0.05080	2.24	0.28743	2.72	0.0410	1.55	256.5	6.2	259.2	3.9
PZH15-03-13	636	454	0.713	0.07	0.05142	1.01	0.28878	1.94	0.0407	1.66	257.6	4.4	257.4	4.2
PZH15-03-14	376	342	0.908	0.16	0.05129	1.29	0.29717	2.31	0.0420	1.92	264.2	5.4	265.3	5.0
PZH15-03-15	234	229	0.978	0.30	0.05185	1.65	0.29315	2.24	0.0410	1.52	261.0	5.2	259.1	3.9
Zircon from the Hongge clinopyroxenite (N26°38.054′, E101°59.321′, H 1679 m)														
HG15-03-1	884	946	1.071	0.17	0.05090	1.28	0.28101	2.02	0.0400	1.56	251.5	4.5	253.1	3.9
HG15-03-3	2210	2722	1.232	0.04	0.05134	0.67	0.28930	1.65	0.0409	1.50	258.0	3.8	258.2	3.8
HG15-03-4	1439	2058	1.430	0.06	0.05168	1.11	0.29876	1.87	0.0419	1.50	265.4	4.4	264.8	3.9
HG15-03-5	1004	1121	1.116	0.33	0.05070	1.36	0.28704	2.08	0.0411	1.57	256.2	4.7	259.4	4.0
HG15-03-6	1481	1710	1.155	0.07	0.05146	0.87	0.29110	1.78	0.0410	1.56	259.4	4.1	259.2	4.0
HG15-03-9	1058	849	0.803	0.08	0.05131	0.92	0.28932	1.95	0.0409	1.72	258.0	4.5	258.4	4.4
HG15-03-10	1037	1127	1.087	0.10	0.05088	0.94	0.28632	2.00	0.0408	1.77	255.7	4.5	257.9	4.5
HG15-03-11	1315	1601	1.218	0.09	0.05149	1.01	0.28708	1.96	0.0404	1.68	256.3	4.4	255.5	4.2
HG15-03-2	973	866	0.889	4.01	0.05034	9.40	0.28275	9.57	0.0407	1.78	252.8	21.6	257.4	4.5
HG15-03-7	199	136	0.684	0.05	0.13923	0.61	7.65690	1.62	0.3989	1.50	2191.6	14.7	2163.8	27.7
HG15-03-8	357	153	0.428	0.07	0.06618	0.79	1.22029	1.78	0.1337	1.60	809.9	10.0	809.1	12.2
HG15-03-12	205	88	0.429	0.07	0.11075	0.55	4.97962	1.64	0.3261	1.55	1815.9	14.0	1819.4	24.6
HG15-03-13	1181	896	0.759	7.08	0.07891	34.14	0.44930	34.29	0.0413	3.13	376.8	114.1	260.9	8.0
HG15-03-14	252	437	1.733	1.51	0.07527	1.50	1.86742	2.13	0.1799	1.50	1069.6	14.2	1066.6	14.8
HG15-03-15	215	228	1.064	0.12	0.12579	0.51	6.31810	1.59	0.3643	1.51	2021.0	14.1	2002.5	26.1
Zircon from the Taihe gabbro (N27°54.437′, E102°08.247′, H 1620 m)														
TH15-03-1	1058	1247	1.179	0.08	0.05153	0.89	0.28951	1.85	0.0407	1.62	258.2	4.2	257.4	4.1
TH15-03-2	1181	1564	1.324	0.09	0.05127	1.01	0.29592	1.81	0.0419	1.51	263.2	4.2	264.4	3.9
TH15-03-3	801	898	1.120	0.10	0.05130	1.14	0.29039	2.09	0.0411	1.75	258.9	4.8	259.4	4.5
TH15-03-4	605	386	0.639	0.23	0.05195	1.02	0.29918	1.99	0.0418	1.72	265.8	4.7	263.8	4.4
TH15-03-5	1384	1811	1.309	0.09	0.05139	0.69	0.30164	1.77	0.0426	1.63	267.7	4.2	268.7	4.3
TH15-03-6	848	948	1.118	0.09	0.05159	0.89	0.29180	1.77	0.0410	1.53	260.0	4.1	259.2	3.9
TH15-03-7	889	942	1.060	0.08	0.05155	1.34	0.29894	2.12	0.0421	1.64	265.6	5.0	265.6	4.3
TH15-03-8	712	474	0.666	0.17	0.05110	1.50	0.28474	2.12	0.0404	1.50	254.4	4.8	255.4	3.8

(*continued on next page*)

Table 1 (*continued*)

Sample/spot	U (ppm)	Th (ppm)	Th/U	f_{206} (%)	$^{207}Pb/^{206}Pb$	1σ (%)	$^{207}Pb/^{235}U$	1σ (%)	$^{206}Pb/^{238}U$	1σ (%)	$^{207}Pb/^{235}U$ age (Ma)	1σ	$^{206}Pb/^{238}U$ age (Ma)	1σ
TH15-03-9	1945	3965	2.039	0.33	0.05127	1.19	0.30397	1.98	0.0430	1.58	269.5	4.7	271.4	4.2
TH15-03-11	558	567	1.017	0.26	0.05084	1.46	0.28990	2.12	0.0414	1.54	258.5	4.9	261.2	3.9
TH15-03-12	769	836	1.088	0.10	0.05152	0.91	0.30382	1.76	0.0428	1.51	269.4	4.2	270.0	4.0
TH15-03-13	1952	1855	0.950	0.04	0.05166	0.62	0.29961	1.65	0.0421	1.53	266.1	3.9	265.6	4.0
TH15-03-14	928	923	0.994	0.14	0.05135	1.11	0.29525	1.95	0.0417	1.61	262.7	4.5	263.4	4.1
TH15-03-15	998	1251	1.254	0.16	0.05117	1.10	0.29523	1.90	0.0418	1.55	262.7	4.4	264.3	4.0
Measured values for the Qinghu zircon standard														
Qinghu-1	2219	1227	0.553	0.14	0.04840	1.12	0.16768	1.90	0.0251	1.54	157.4	2.8	160.0	2.4
Qinghu-2	703	344	0.489	0.16	0.04888	1.22	0.16779	1.94	0.0249	1.50	157.5	2.8	158.5	2.4
Qinghu-3	1194	726	0.608	0.09	0.04913	0.96	0.17101	1.80	0.0252	1.52	160.3	2.7	160.7	2.4
Qinghu-4	2528	778	0.308	0.04	0.04892	0.72	0.16857	1.68	0.0250	1.52	158.2	2.5	159.1	2.4
Recommended values for the Qinghu standard (Li et al., 2013)														
Qinghu													159.5	0.2

Note: $f_{206} = (^{204}Pb/^{206}Pb)m * (^{206}Pb/^{204}Pb)c$, with $(^{204}Pb/^{206}Pb)m$ the measured $^{204}Pb/^{206}Pb$ ratio corrected for background, and $(^{206}Pb/^{204}Pb)c$ the common Pb ratio of the analyzed area, calculated from its U-Pb age.

zones: namely the Lower, Middle and Upper Zones (Fig. 2a–c). The samples for zircon O-Hf isotope analyses were all collected from the oxide ore-bearing zones of these intrusions, immediately below an oxide ore layer at Panzhihua (Fig. 2a), between two oxide ore layers at Hongge (Fig. 2b), and in the upper part of the Middle Zone at Taihe (Fig. 2c).

The gabbro sample (PZH15-03) from the Panzhihua intrusion is relatively fresh, and contains <5% olivine, 40–45% pyroxenes, 40–50% plagioclase, and minor hornblende and Fe-Ti oxides (Fig. 3a, b). The clinopyroxenite sample (HG15-03) from the Hongge intrusion contains <5% olivine, 50–60% clinopyroxenite, 5–10% Fe-Ti oxides, <5% apatite, and minor amounts of plagioclase, hornblende, and phlogopite (Fig. 3c, d). The gabbro sample (TH15-03) from the Taihe intrusion contains <5% olivine, 30–40% pyroxenes, 40–45% plagioclase, 5–10% Fe-Ti oxides, and minor hornblende and phlogopite (Fig. 3e, f). Partial alteration of clinopyroxene to chlorite, and plagioclase to sericite + epidote + albite is slightly more severe in the samples from the Hongge and Taihe intrusions than in the sample from the Panzhihua intrusion.

3.2. Analytical methods

3.2.1. Zircon U-Pb ages and oxygen isotopes

In-situ O isotope analysis and U-Pb dating of zircon were conducted using a CAMECA IMS-1280HR SIMS (secondary ion mass spectrometry) instrument at the Institute of Geology and Geophysics, Chinese Academy of Sciences, Beijing. O isotopes of zircon crystals in a polished epoxy disc were measured first. The disc was then polished again for zircon U-Pb analysis.

The analytical procedures and operating conditions for zircon O isotope measurement are the same as those given in Li et al. (2010a). The instrumental mass fractionation (IMF) of O isotopes was corrected using an internal zircon standard, the Penglai zircon with a recommended $\delta^{18}O_{VSMOW}$ of 5.31 ± 0.10‰ (Li et al., 2010b), following the procedures of Li et al. (2010a). The Qinghu zircon standard, which has a recommended $\delta^{18}O$ value of 5.4 ± 0.2‰ (Li et al., 2013), was used as secondary standard. The measured and recommended $\delta^{18}O$ values of the secondary standard agree with each other well (Table 1).

The analytical procedures and data processing of zircon U-Pb dating are the same as those given in Li et al. (2009). Correction to common lead was made using the measured ^{204}Pb and the model crustal Pb isotope compositions (Stacey and Kramers, 1975). The Qinghu zircon standard ($^{206}Pb/^{238}U$ age = 159.5 ± 0.2 Ma, Li et al., 2013) was used as a secondary standard. The results from this study and the recommended age of the secondary standard agree with each other well (Table 2). Plotting and age calculations were done using the Isoplot v.3.75 of Ludwig (2012).

3.2.2. Zircon Hf isotopes

In-situ zircon Hf isotope analysis were performed using a Neptune Plus multi-collector ICP-MS equipped with a GeoLasPro HD excimer ArF laser-ablation sampling system in the laboratory of the Wuhan Sample Solution Ana-

Table 2
Zircon Lu-Hf and O isotope data for the Hongge, Panzhihua and Taihe intrusions.

Sample/spot	$^{176}Yb/^{177}Hf$	$^{176}Lu/^{177}Hf$	$^{176}Hf/^{177}Hf$	1σ	$(^{176}Hf/^{177}Hf)_i$	$\varepsilon_{Hf}(t)$	$\delta^{18}O$ (‰)	2σ
Zircon from the Panzhihua gabbro								
PZH15-03-01	0.037338	0.001113	0.282783	0.000020	0.282777	5.82	5.49	0.30
PZH15-03-02	0.011095	0.000340	0.282744	0.000018	0.282742	4.60	6.10	0.30
PZH15-03-03	0.055393	0.001611	0.282773	0.000022	0.282765	5.39	6.07	0.16
PZH15-03-04	0.016702	0.000512	0.282773	0.000019	0.282770	5.57	5.70	0.26
PZH15-03-05	0.013083	0.000421	0.282747	0.000018	0.282745	4.64	5.86	0.22
PZH15-03-06	0.021234	0.000647	0.282768	0.000021	0.282765	5.33	5.84	0.19
PZH15-03-07	0.010040	0.000316	0.282760	0.000017	0.282759	5.22	5.87	0.21
PZH15-03-08	0.020670	0.000732	0.282766	0.000020	0.282763	5.37	5.64	0.24
PZH15-03-09	0.024652	0.000736	0.282776	0.000021	0.282773	5.65	5.92	0.21
PZH15-03-10	0.031350	0.000930	0.282777	0.000021	0.282772	5.61	5.80	0.24
PZH15-03-11	0.026239	0.000792	0.282784	0.000022	0.282780	5.96	5.86	0.26
PZH15-03-12	0.016098	0.000523	0.282793	0.000020	0.282790	6.33	5.72	0.26
PZH15-03-13	0.027085	0.000823	0.282792	0.000019	0.282788	6.22	5.99	0.20
PZH15-03-14	0.015550	0.000466	0.282750	0.000020	0.282747	4.96	5.81	0.23
PZH15-03-15	0.018700	0.000556	0.282764	0.000018	0.282762	5.32	5.76	0.21
Zircon from the Hongge clinopyroxenite								
HG15-03-01	0.017601	0.000477	0.282712	0.000023	0.282710	3.35	5.97	0.21
HG15-03-03	0.014940	0.000405	0.282718	0.000023	0.282716	3.68	5.97	0.27
HG15-03-04	0.050532	0.001497	0.282746	0.000029	0.282739	4.64	6.45	0.17
HG15-03-05	0.027843	0.000781	0.282707	0.000025	0.282704	3.28	6.32	0.21
HG15-03-06	0.027924	0.000777	0.282705	0.000028	0.282702	3.20	6.40	0.26
HG15-03-09	0.026128	0.000758	0.282702	0.000025	0.282699	3.08	5.77	0.31
HG15-03-10	0.026804	0.000780	0.282711	0.000024	0.282707	3.37	6.20	0.11
HG15-03-11	0.041277	0.001110	0.282718	0.000027	0.282713	3.53	6.32	0.21
HG15-03-13	0.056375	0.001790	0.282751	0.000023	0.282742	4.68		
Zircon from the Taihe gabbro								
TH15-03-01	0.085295	0.001964	0.282899	0.000018	0.282889	9.81		0.13
TH15-03-02								0.24
TH15-03-03	0.120410	0.002801	0.282899	0.000022	0.282885	9.69	4.15	0.25
TH15-03-04	0.064705	0.001571	0.282878	0.000019	0.282871	9.28	4.47	0.37
TH15-03-05							4.46	0.16
TH15-03-06							4.12	0.26
TH15-03-07							4.56	0.26
TH15-03-08	0.082232	0.001693	0.282865	0.000029	0.282857	8.60	4.23	0.10
TH15-03-09	0.105102	0.002054	0.282870	0.000032	0.282860	9.07	4.34	0.37
TH15-03-11							4.22	0.24
TH15-03-12	0.084984	0.001738	0.282848	0.000027	0.282839	8.30	4.19	0.30
TH15-03-13	0.100222	0.002013	0.282856	0.000028	0.282846	8.44		0.23
TH15-03-14							4.44	0.16
TH15-03-15							4.42	0.26
Measured values for the secondary standards								
Qinghu-1							5.28	0.29
Qinghu-2							5.53	0.16
Qinghu-3							5.34	0.21
Qinghu-4							5.40	0.28
Qinghu-5							5.29	0.34
Qinghu-6							5.66	0.20
TEM	0.044438	0.001288	0.282721	0.000010				
TEM	0.046562	0.001435	0.282688	0.000015				
TEM	0.067353	0.001849	0.282681	0.000015				
TEM	0.043244	0.001146	0.282702	0.000013				
GJ-1	0.007855	0.000249	0.282021	0.000010				
GJ-1	0.007928	0.000247	0.282010	0.000014				
GJ-1	0.008039	0.000254	0.282038	0.000015				
GJ-1	0.008053	0.000250	0.282021	0.000010				
Recommended values for the secondary standards								
Qinghu (Li et al., 2013)							5.40	0.20
TEM (Wu et al., 2006)			0.282680	0.000031				
GJ-1 (Morel et al., 2008)			0.282000	0.000005				

Table 3
Rb-Sr and Sm-Nd isotope data for the Hongge, Panzhihua and Taihe Fe-Ti-V oxide ore-bearing mafic–ultramafic intrusions.

Sample	Rock type	Rb	Sr	$^{87}Rb/^{86}Sr$	$^{87}Sr/^{86}Sr$	1σ	Sm	Nd	$^{147}Sm/^{144}Nd$	$^{143}Nd/^{144}Nd$	1σ	$(^{87}Sr/^{86}Sr)_i$	ε_{Nd} (t)
PZH15-02	Gabbro	11.4	599	0.055048	0.704878	0.000005	3.06	12.5	0.147997	0.512672	0.000009	0.704674	2.28
PZH15-03	Gabbro	11.5	1030	0.032295	0.705226	0.000006	2.27	9.58	0.143252	0.512667	0.000011	0.705107	2.34
TH15-02	Gabbro	7.28	612	0.034408	0.705311	0.000004	3.23	13.6	0.143584	0.512681	0.000016	0.705184	2.60
TH15-03	Gabbro	13.8	1340	0.029788	0.704988	0.000004	5.06	20.4	0.149956	0.512679	0.000008	0.704878	2.35
HG15-02	Clinopyroxenite	4.49	142	0.091461	0.705124	0.000006	2.89	11.8	0.148067	0.512671	0.000013	0.704786	2.26
HG15-03	Clinopyroxenite	38.4	1510	0.073559	0.705272	0.000006	17.3	80.1	0.130574	0.512687	0.000011	0.705000	3.15
Measured values for the secondary standards													
NIST SRM987				0.000029	0.710232	0.000003							
NIST SRM987				0.000192	0.710255	0.000006							
JNdi-1									0.000005	0.512098	0.000007		
JNdi-1									0.000005	0.512092	0.000005		
Recommended values for the secondary standards													
NIST SRM987 (Thirlwall, 1991)					0.710241	0.000006							
JNdi-1 (Tanaka et al., 2000)										0.512112	0.000007		

Notes: ε_{Nd} is the derivation in parts per 10,000 of the initial ratio from that of a chondritic reservoir at the crystallization age of 260 Ma for the Hongge, Panzhihua and Taihe intrusions.

lytical Technology Co., Ltd., Wuhan, China. The detailed analytical procedures and operation conditions are the same as those given in Hu et al. (2012). Prior to sample analysis, 20–30 s of stationary collection of background intensity was collected. A zircon grain was then ablated for 30 s by a laser beam with the energy density of 15 J/cm^2 and spot size of 50 μm in diameter. Helium was used as the carrier gas. $^{176}Lu/^{175}Lu$ of 0.02658 and $^{176}Yb/^{173}Yb$ of 0.796218 were used to correct the isobaric interferences of ^{176}Lu and ^{176}Yb on ^{176}Hf, respectively. For instrumental mass bias correction the measured Yb and Hf isotope ratios were normalized to $^{172}Yb/^{173}Yb = 1.35274$ and $^{179}Hf/^{177}Hf = 0.7325$, respectively, using an exponential law. The mass bias behavior of Lu was assumed to follow that of Yb. The 91,500 zircon standard ($^{176}Hf/^{177}Hf = 0.282313 \pm 8$, Blichert-Toft, 2008) was used as primary calibration standard. The TEM (Wu et al., 2006) and GJ-1 (Morel et al., 2008) zircon standards were used as secondary standards. The measured and recommended values of the secondary standards agree with each other well (Table 2).

3.2.3. Whole-rock Sr-Nd isotopes

Sample powders used for Rb-Sr and Sm-Nd isotope analysis were spiked with mixed isotope tracers, dissolved in Teflon capsules using HF and HNO_3 acids, and separated using conventional cation-exchange techniques. The Sr and Nd isotopes of the samples were determined using Neptune Plus MC-ICP-MS in the State Key Laboratory of Ore Deposit Geochemistry, Institute of Geochemistry, Chinese Academy of Sciences, Guiyang, China. Mass fractionation corrections for Sr and Nd isotopic ratios are based on $^{86}Sr/^{88}Sr = 0.1194$ and $^{146}Nd/^{144}Nd = 0.7219$, respectively. The NIST SRM987 and JNdi-1 standards were used as secondary standards. The measured and true values of the secondary standards are given in Table 3, and closely agree.

4. RESULTS

4.1. Zircon U-Pb ages

The U-Pb data of zircon grains separated from the Panzhihua gabbro, Hongge clinopyroxenite and Taihe gabbro are listed in Table 1. The cathodoluminescence (CL) images of the analyzed zircon crystals are shown in Fig. 4. They are euhedral to subhedral grains or fragments with either a broad zoning or a homogeneous nature, which are common for gabbroic rocks worldwide (Corfu et al., 2003). Zircons crystallizing in mafic magma occur interstitially to other minerals, and commonly exhibit partial crystal faces or subhedral morphology (e.g., Scoates and Chamberlain, 1995).

The grain sizes of zircon from the Panzhihua, Hongge and Taihe intrusions are from 50 to 150 μm long, with length-to-width ratios of 1:1–2:1. The zircon grains from the Panzhihua gabbro are colorless and transparent or brown and semi-transparent. In contrast, those from the Hongge clinopyroxenite and Taihe gabbro are all brown and semi-transparent. The change in color is apparently

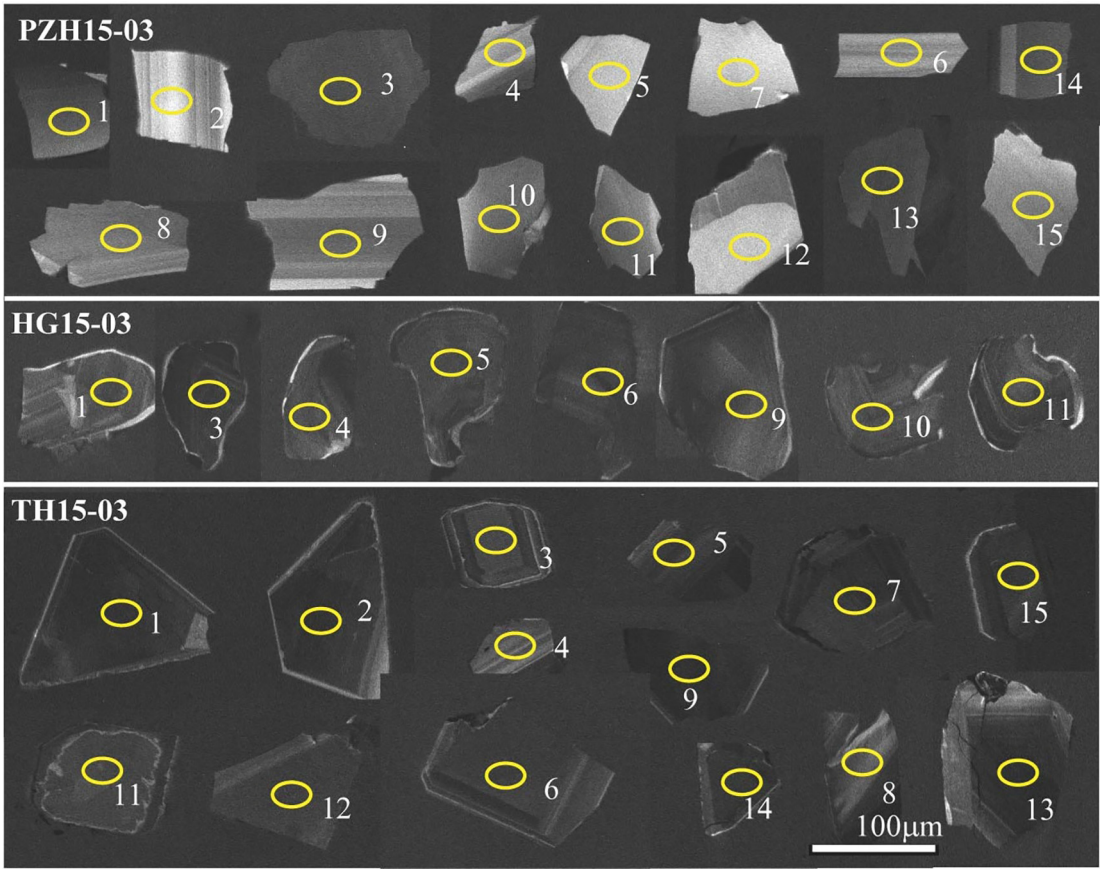

Fig. 4. Cathodoluminescence images of zircon crystals from the Panzhihua, Hongge and Taihe intrusions, with $^{206}Pb/^{238}U$ ages in Ma.

related to the variations of U and Th contents. The colorless-transparent zircons from the Panzhihua gabbro (grain #2, 4, 5, 6, 7, 12 and 15) contain 116–209 ppm U and 74–229 ppm Th, with Th/U ratios from 0.55 to 0.98 (Table 1). In contrast, the concentrations of these elements in the brown-semi transparent zircons from the Panzhihua gabbro (grain #1, 3, 8, 9, 10, 11, 13 and 14) are higher, varying from 304 to 687 ppm for U and from 128 to 901 ppm Th, with a larger range of Th/U ratios from 0.42 to 1.31 (Table 1). The zircons from the Hongge clinopyroxenite and Taihe gabbro are generally darker (Fig. 4) and contain higher U and Th than those from the Panzhihua gabbro (Table 1). The concentrations of U and Th in the zircons from the Hongge clinopyroxenite (grain #1, 3, 4, 5, 6, 9, 10 and 11) and Taihe gabbro are similarly high, varying from 605 to 2210 ppm for U and from 386 to 3965 ppm for Th, with Th/U ratios from 0.64 to 2.04 (Table 1).

The SIMS-determined U-Pb isotopic compositions of 15 zircon grains from the Panzhihua gabbro yield a Concordia age of 257.6 ± 2.1 Ma (Fig. 5a). Our new zircon U-Pb age for the Panzhihua intrusion is within the range of the ages previously-reported for this intrusion by the LA-ICP-MS method (255.4 ± 3.1 Ma and 257.9 ± 2.4 Ma; Zhong et al., 2011a) and by the SHRIMP method (263 ± 3 Ma; Zhou et al., 2005). The SIMS-determined U-Pb isotopic compositions of 8 zircon grains from the Hongge clinopyroxenite yield a Concordia age of 258.2 ± 2.8 Ma (Fig. 5b), which is indistinguishable with the ages previously-reported for this intrusion by the LA-ICP-MS method (258.9 ± 2.1 Ma and 258.7 ± 2.0 Ma; Zhong et al., 2011a) and by the TIMS method (259.3 ± 1.3 Ma; Zhong and Zhu, 2006). The older, xenocrystic zircon grains from the Hongge intrusion have $^{206}Pb/^{238}U$ ages varying from 809.1 Ma to 2163.8 Ma (Table 1). The SIMS-determined U-Pb isotopic compositions of 14 zircon grains from the Taihe gabbro yield a Concordia age of 263.3 ± 2.2 Ma (Fig. 5c), which is within the range of the previously-reported zircon U-Pb ages for the Taihe intrusion determined using the LA-ICP-MS method (264.3 ± 2.5 Ma and 258.8 ± 2.3 Ma; Shellnutt et al., 2011; Zhong et al., 2011a) and by the SHRIMP method (259 ± 3 Ma and 257 ± 4 Ma; She et al., 2014).

4.2. Zircon Hf-O isotopes

The Hf isotope compositions of the dated co-magmatic zircon grains from the Panzhihua, Hongge and Taihe intrusions are listed in Table 2. The $\varepsilon_{Hf}(t)$ values were calculated using the zircon U-Pb ages given in Fig. 5. The $\varepsilon_{Hf}(t)$ values of the dated zircons from the Panzhihua gabbro and Hongge clinopyroxenite are from 4.6 to 6.3 (average of 5.5), and from 3.1 to 4.7 (average of 3.6), respectively. In contrast, the $\varepsilon_{Hf}(t)$ values of the dated zircons from the Taihe gabbro

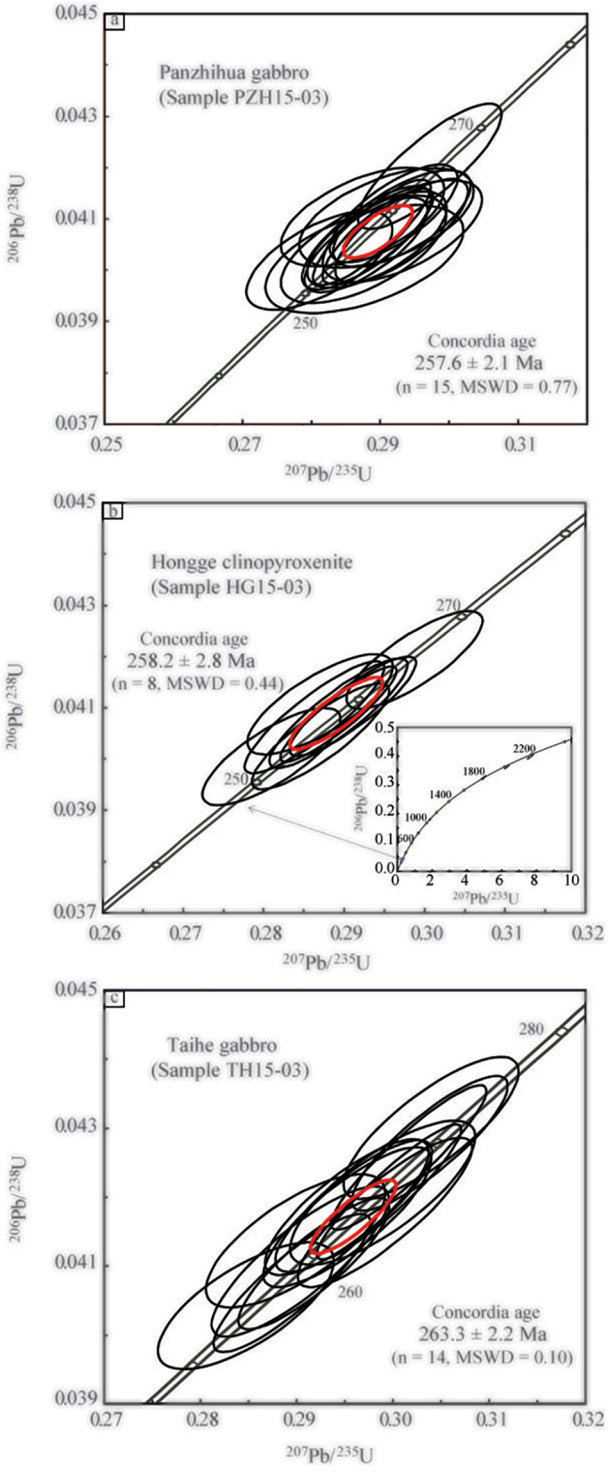

Fig. 5. Concordia U-Pb isotope age diagrams of zircon crystals from the Panzhihua, Hongge and Taihe intrusions.

are significantly higher, ranging from 8.3 to 9.8, with an average of 9.0. A comparison between our new results and the previous data for these intrusions from Shellnutt et al. (2011) and Zhong et al. (2011a) is illustrated in Fig. 6a. The results from the different studies are generally in good agreement and show significantly higher zircon $\varepsilon_{Hf}(t)$ values for the Taihe intrusion than the Panzhihua and Hongge intrusions. The zircon $\varepsilon_{Hf}(t)$ values for the magmatic Fe-Ti-V oxide deposits plot between the chondritic uniform reservoir and the growth curve of depleted mantle, and are all higher than those of a coeval magmatic Ni-Cu sulfide deposit, i.e., the Zhubu deposit in the Emeishan LIP (Fig. 6a).

The $\delta^{18}O$ values of the dated zircons from the Panzhihua gabbro, Hongge clinopyroxenite and Taihe gabbro are also listed in Table 2. The $\delta^{18}O$ values of the Panzhihua zircons are from 5.49 to 6.10‰, with an average of 5.84‰. The $\delta^{18}O$ values of the Hongge zircons are from 5.77 to 6.45‰, with an average of 6.18‰. The $\delta^{18}O$ values of the Taihe zircons are distinctly lower, ranging from 4.12 to 4.56‰, with an average of 4.33‰. The results show that the zircons of the Panzhihua and Hongge intrusions have higher $\delta^{18}O$ values than the mantle zircon values (5.3 ± 0.3‰) of Valley (2003) that are based on the results for zircon megacrysts from kimberlite pipes near Kimberley, South Africa. In contrast, the zircons of the Taihe intrusion all have $\delta^{18}O$ values significantly lower than the mantle zircon values (Fig. 6b). Our combined O-Hf isotopic analyses of a single grain of zircon reveal for the first time that these two different isotopic systems are decoupled in the zircons of the Taihe intrusion, i.e., the zircons have very low $\delta^{18}O$ values and very high $\varepsilon_{Hf}(t)$ values. The former are much lower than the mantle zircon values whereas the latter are close to the depleted mantle values. The significance of this new finding is evaluated below.

It should be mentioned that the $\delta^{18}O$ values of zircons from the Taihe deposit analyzed by us (4.12–4.56‰) are significantly lower than those of clinopyroxene separates from the same deposit (5.1–6.9‰) analyzed by Yu et al. (2015). One possibility for the difference is due to different samples used by the different studies. Another possibility is due to the different effects of low-temperature hydrothermal alteration on the different phases. As pointed out by Valley (2003), the primary $\delta^{18}O$ values of parental magmas are commonly much better preserved in magmatic zircons than some rock-forming minerals such as clinopyroxene and plagioclase in low-temperature hydrothermally-altered mafic rocks. As acknowledged by Yu et al. (2015), the high $\delta^{18}O$ values of clinopyroxene from the Taihe deposit acquired by them could be due to interaction with evolved, ^{18}O enriched meteoric water at low temperatures.

4.3. Sr-Nd isotopes

The whole-rock Rb-Sr and Sm-Nd data of the samples from the Panzhihua, Hongge and Taihe intrusions used in this study are given in Table 3. The calculated $(^{87}Sr/^{86}Sr)_i$ ratios (t = 260 Ma) are from 0.7047 to 0.7051 for the Panzhihua gabbros, from 0.7048 to 0.7050 for the Hongge clinopyroxenites, and from 0.7049 to 0.7052 for the Taihe gabbros. The calculated $\varepsilon_{Nd}(t)$ values for the samples from these three intrusions are from 2.28 to 2.34, from 2.26 to 3.15, and from 2.35 to 2.60, respectively. A comparison between our new results and the previous data for these three intrusions (Zhong et al., 2003; Zhang et al., 2009; Hou et al., 2012; Howarth and Prevec, 2013; Song et al.,

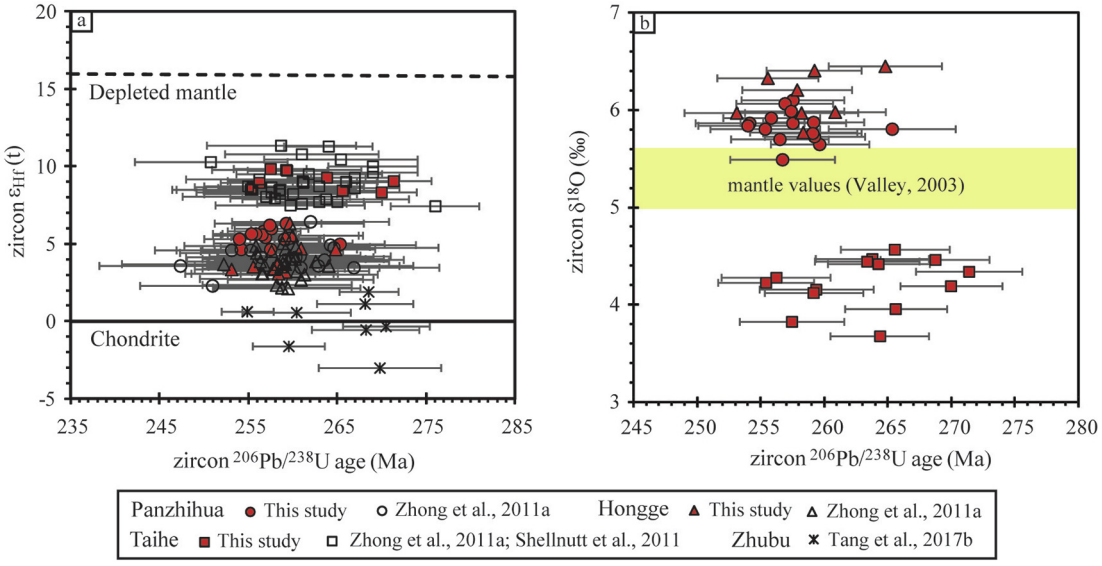

Fig. 6. Plots of $\varepsilon_{Hf}(t)$ versus crystallization age (a), and $\delta^{18}O$ versus crystallization age (b).

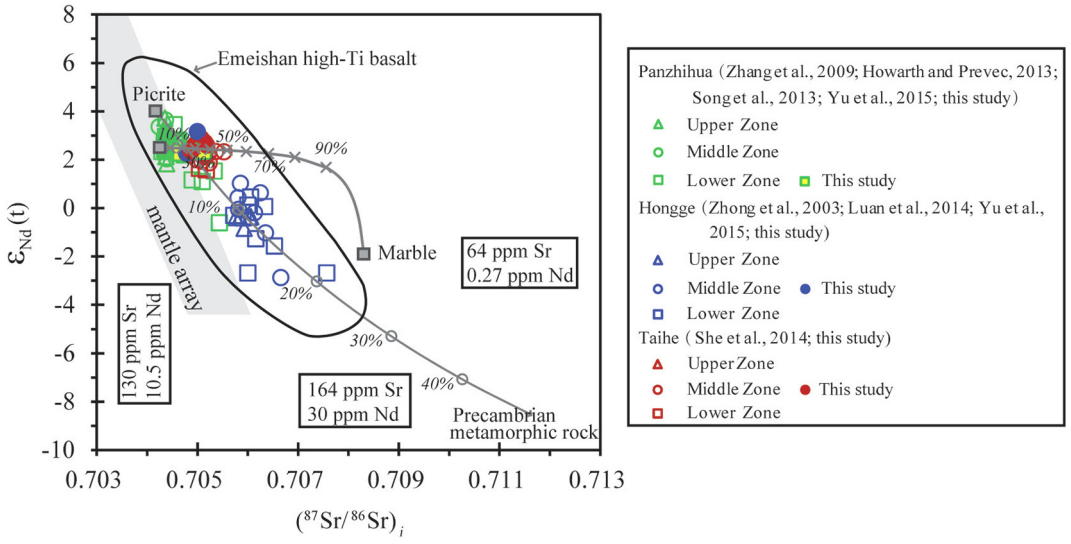

Fig. 7. Plot of whole-rock ε_{Nd} versus $(^{87}Sr/^{86}Sr)_i$ for the Panzhihua, Hongge and Taihe intrusions. The mantle Sr-Nd isotope array is from DePaolo and Wasserburg (1979). The field for the Emeishan high-Ti basalts is based on the data from Xu et al. (2001), Xiao et al. (2004) and Zhang et al. (2008). The Sr-Nd isotope compositions of the Emeishan picrite for modeling are the average of two picrite samples with the lowest Nd contents from Chung and Jahn (1995) and Zhang et al. (2006). The concentrations of Sr and Nd and the Sr and Nd isotope compositions of the Precambrian metamorphic rock from Gao et al. (1999), Zhang et al. (2008), Luan et al. (2014) and Yu et al. (2015) The concentrations of Sr and Nd in the marble are from Ganino et al. (2008); the Sr and Nd isotope compositions of the marble are from Ganino et al. (2013b) and Yu et al. (2015).

2013; Luan et al., 2014; She et al., 2014; Yu et al., 2015) is illustrated in Fig. 7. Our new data for the mineralized zones plot in the upper part of the Sr-Nd isotopic array for the Panzhihua, Taihe and Hongge intrusions (Fig. 7).

5. DISCUSSION

It is widely accepted that the Fe-Ti-V oxide ore deposits in the Emeishan LIP are related to high-Ti basalts, but the role of crustal contamination and mantle source variation are still debated (e.g., Zhou et al., 2005; Ganino et al., 2008, 2013a, 2013b; Zhong et al., 2011b; Hou et al., 2012; Bai et al., 2014; Yu et al., 2015; Tang et al., 2017a). Such debate is difficult to resolve using a single isotope tracer. A combination of zircon Lu-Hf isotope systematics and O isotopes is more robust, because it is less common for the different reservoirs to have the same Hf-O isotope ratios relative to ratios obtained from just one of these elements (Valley, 2003; Vervoort and Kemp, 2016).

In mafic magma, zircon saturation is only reached late in the crystallization history (Hanchar and Watson, 2003). Such zircons commonly occur interstitially to other miner-

als in gabbroic rocks (e.g., Scoates and Chamberlain, 1995). In such rocks zircon Hf-O isotopes directly track the isotopic compositions of the interstitial liquids rather than the primary mantle-derived magma. It is likely that the interstitial liquids were contaminated with crustal materials during magma ascent, storage and crystallization. Thus, potential crustal contamination must be assessed before the isotope data can be used to evaluate any mantle source variation. With this in mind, we begin with whole-rock Sr-Nd isotopes and then move to zircon Hf-O isotopes in the discussion below.

5.1. Crustal contamination

Previous studies have shown that the parental magmas of the Panzhihua, Hongge and Taihe intrusions were contaminated by crustal materials (e.g., Howarth and Prevec, 2013; Luan et al., 2014; Yu et al., 2015). As shown in Fig. 7, the Sr-Nd isotope compositions of the Hongge intrusion plot between the Precambrian metamorphic rock in the region and the uncontaminated high-Ti picrites of the Emeishan LIP. The uncontaminated isotopic compositions of the picrites are inferred from the similarity with the mantle array of DePaolo and Wasserburg (1979). The Sr-Nd isotope variations of the Hongge intrusion are generally consistent with parental magmas being variably contaminated with up to 20 wt.% Precambrian metamorphic rock (Fig. 7). The Lower Zone of the Panzhihua intrusion, which hosts the major Fe-Ti-V oxide ore layers (Fig. 2a), has larger ranges of $\varepsilon_{Nd}(t)$ and $(^{87}Sr/^{86}Sr)_i$ than the Middle and Upper Zones of this intrusion (Zhang et al., 2009; Howarth and Prevec, 2013; Song et al., 2013; Yu et al., 2015; this study). The samples with lower $\varepsilon_{Nd}(t)$ and higher $(^{87}Sr/^{86}Sr)_i$ from the ore-bearing zone of the Panzhihua intrusion are consistent with up to 10 wt.% Precambrican metamorphic rock contamination in the parental magma. The ore-bearing zone (Middle Zone) and the ore-barren zone (Lower Zone) of the Hongge intrusion (Fig. 2b) have similar large ranges of $(^{87}Sr/^{86}Sr)_i$ and $\varepsilon_{Nd}(t)$ values, which are consistent with variable degrees of crustal contamination at scales that are smaller than a single zone (Fig. 7). The Upper Zone of this intrusion has tighter ranges of $(^{87}Sr/^{86}Sr)_i$ (0.7058 to 0.7060) and $\varepsilon_{Nd}(t)$ (−0.84 to −0.36) values than those of the other zones (Fig. 7).

Except for two samples from the Middle Zone of the Taihe intrusion, up to 30% contamination with marble can explain the observed Sr-Nd isotope variation in the parental magmas for the Panzhihua and Taihe intrusions (Fig. 7). Unlike the Panzhihua intrusion, marble wall-rock is rare for the Taihe intrusion (Fig. 2a, c). Thus, marble contamination in the Taihe magma likely took place at depth, which is consistent with the presence of entrained marble xenoliths in this intrusion in some places (Panxi Geological Unit, 1984). It is important to note that the $\varepsilon_{Nd}(t)$ and $(^{87}Sr/^{86}Sr)_i$ of our samples from the ore-bearing zone (Middle Zone) of the Hongge intrusion are similar to those of our samples from the ore-bearing zones of the Panzhihua and Taihe intrusions, implying that the parental magma for the ore-bearing zone of the Hongge intrusion may have also experienced marble assimilation (Fig. 7). However, given the fact that there are no marble wall-rocks nor marble xenoliths in the Hongge intrusion (Fig. 2b), such interpretation is highly speculative. Moreover, there is really no need to call upon such a process, as the Sr-Nd isotope array of this intrusion can be well explained by contamination with Precambrian metamorphic wall-rocks (Fig. 7).

5.2. Origin of zircon Hf-O isotope decoupling in the Taihe deposit

The zircon grains from the Taihe deposit have high $\varepsilon_{Hf}(t)$ values from 8.3 to 9.8; the zircon grains from the Panzhihua deposit have intermediate $\varepsilon_{Hf}(t)$ values from 4.6 to 6.3; the zircon grains from the Hongge deposit have relatively low $\varepsilon_{Hf}(t)$ values from 3.1 to 4.7 (Fig. 6a). A decrease of zircon $\varepsilon_{Hf}(t)$ values from the Taihe and Panzhihua deposits to the Honnge deposit can be explained by decreasing degrees of contamination with the Precambrian metamorphic rock in the parental magmas. Such an interpretation is also supported by the whole-rock Sr-Nd isotopes (Fig. 7). However, this type of contamination cannot explain the observed zircon $\delta^{18}O$ differences between these deposits. The zircon $\delta^{18}O$ values of the Taihe deposit are lower than the mantle zircon values ($5.3 \pm 0.3‰$, Valley, 2003) whereas those of the Panzhihua and Hongge deposits are higher than the mantle values (Fig. 6b). Moreover, the zircon grains of the Taihe deposit have higher $\varepsilon_{Hf}(t)$ values but lower $\delta^{18}O$ values than the Panzhihua and Hongge deposits (Fig. 6a, b). Potential contaminants in the region, such as the Precambrian metamorphic rock and marbles, are characterized by higher $\delta^{18}O$ and lower $\varepsilon_{Hf}(t)$ (inferred from Nd isotopes) than the mantle values (Ganino et al., 2013b; Yu et al., 2015). Contamination with these rocks would have resulted in an increase of $\delta^{18}O$ and a decrease of $\varepsilon_{Hf}(t)$ in the contaminated magmas, which is seen in the zircons from the Panzhihua and Hongge deposits but not in those from the Taihe deposit.

The unusual combination of low $\delta^{18}O$ (significantly lower than the mantle value) coupled by very high $\varepsilon_{Hf}(t)$ (similar to the depleted mantle values) for the zircons of the Taihe deposit, which we refer to as zircon Hf-O isotope decoupling for convenience, may be due to contamination with crustal rocks that have very low $\delta^{18}O$ and mantle-like $\varepsilon_{Hf}(t)$ values. However, this type of rock is not present or has not been found in the vicinity of the Taihe deposit (Fig. 2c). It is true that Neoproterozoic granitic rocks with low $\delta^{18}O$ values (~4.2, Zheng et al., 2007) are present in the adjacent region to the northwest of the Taihe deposit, but these rocks are not the required contaminants. The original $\varepsilon_{Hf}(t)$ values of these rocks are from 3.5 to 9.1 (Zheng et al., 2007). By the time the Taihe magmas were emplaced into the crust at ~260 Ma, the $\varepsilon_{Hf}(t)$ values of the Neoproterozoic granitic rocks would have decreased to be between −1.4 and −6.0 due to radiogenic growth through time. Contamination of mantle-derived magma with such rocks would have resulted in lower $\delta^{18}O$ and lower $\varepsilon_{Hf}(t)$ in the contaminated magma, contrary to the results from the

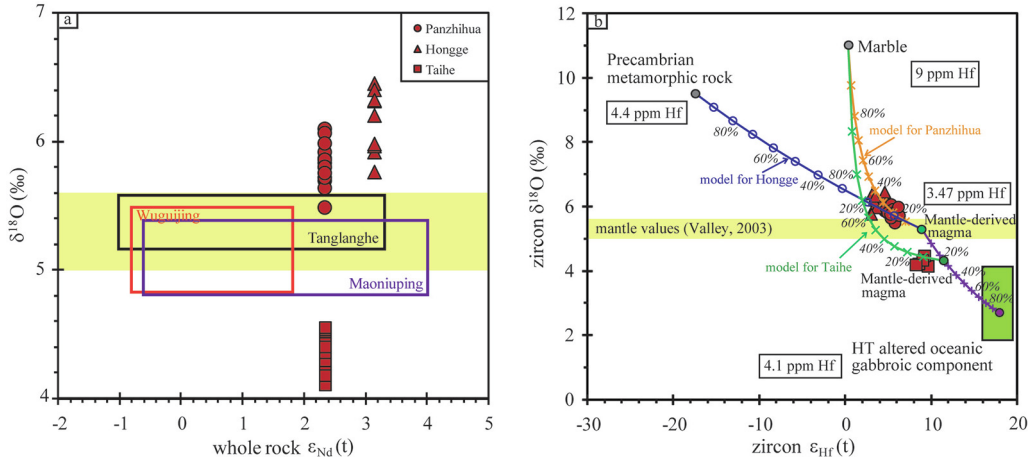

Fig. 8. Plot of mineral (zircon or olivine) $\delta^{18}O$ versus whole-rock ε_{Nd}(a), and zircon ε_{Hf}(t) versus $\delta^{18}O$ (b). The yellow band in (a) and (b) represents the mantle zircon value ($\delta^{18}O = 5.3‰ \pm 0.3‰$; Valley, 2003). The compositions of high temperature (HT) altered oceanic gabbroic crust are from Eiler (2001). Modeling parameters: Precambrian metamorphic rock $\varepsilon_{Hf}(t) = -17.39$ and $\delta^{18}O = +9.5‰$; HT altered oceanic gabbroic component $\varepsilon_{Hf}(t) = +18$ and $\delta^{18}O = +2.7‰$; marble $\varepsilon_{Hf}(t) = 9.0$ and $\delta^{18}O = +11‰$ (Valley, 2003; Eiler, 2001; Chauvel et al., 2008; Vervoort et al., 2011; Ganino et al., 2013b; Yu et al., 2015; Chen and Xing, 2016). The concentrations of Hf in the primary magma are from Yu et al. (2017). The average Hf concentration in continental upper crust from Rudnick and Gao (2003) is used to represent the composition of the Precambrian metamorphic rock.

Taihe deposit. Thus, we rule out this type of contamination as the cause for the observed zircon Hf-O isotope decoupling in the Taihe deposit.

5.3. Mantle source variation

The combined whole-rock $\varepsilon_{Nd}(t)$ values and mineral (zircon or olivine) $\delta^{18}O$ values for the Emeishan LIP (Fig. 8a) show that the $\varepsilon_{Nd}(t)$ values of the Panzhihua, Hongge and Taihe intrusions are within the range of the Emeishan picrites that have relatively high Ti contents such as those from the Tanglanghe, Maoniuping and Wuguijing areas (Zhang et al., 2006, 2008; Bai et al., 2013). In contrast, the $\delta^{18}O$ values of the intrusive rocks (Table 2) are either higher or lower than those of the picrites (Yu et al., 2017). The $\delta^{18}O$ values of olivine phenocrysts in the picrites are mainly within the range of typical mantle values (Fig. 8a). The Fo contents of the olivine phenocrysts are mainly between 87 and 91 mol% (Yu et al., 2017). In contrast, the Fo contents of olivine in the intrusions are much lower, mainly between 65 and 70 mol% (Bai et al., 2014). The different olivine compositions between the picrites and the intrusive rocks indicate that the parental magmas for the intrusive rocks are more evolved than those for the picrites due to fractional crystallization and crustal contamination. Fractional crystallization commonly has little effect on the oxygen isotope composition of mafic magma. In contrast, crustal contamination can have a significant effect on the oxygen isotope composition, commonly resulting in an increase of $\delta^{18}O$ values, not a decrease of such values in the contaminated magma, because the average $\delta^{18}O$ value of the crust is typically significantly higher than that of the mantle. Thus, this process can only explain the origin of the parental magmas for the Panzhihua and Hongge deposits, which have higher $\delta^{18}O$ value of zircon than those of typical mantle ($5.3‰ \pm 0.3‰$; Valley, 2003) and the picrites (Fig. 8a), but not the origin of the parental magma for the Taihe deposit, which has significantly lower $\delta^{18}O$ values of zircon than those of typical mantle as well as the picrites (Fig. 8a). Furthermore, as mentioned above, crustal contamination can well explain the coherent zircon Hf-O isotope variations in the Panzhihua and Hongge deposits but cannot explain the zircon Hf-O isotope decoupling in the Taihe deposit. As shown in Fig. 8b, the zircon Hf-O isotope compositions of the Panzhihua and Hongge deposits can be explained by 20 wt.% bulk marble assimilation and 15 wt.% contamination with the Precambrian metamorphic rock, respectively, which are consistent with the results from whole-rock Sr-Nd isotopes (Fig. 7).

Oceanic sediments commonly have much higher $\delta^{18}O$ values than the mantle. Low temperature alteration can increase the $\delta^{18}O$ values of oceanic crust because of large positive isotope fractionation factors between minerals and fluids (Bindeman, 2008). In contrast, high temperature alteration of gabbroic rocks (including MORBs) in an oceanic setting can decrease the $\delta^{18}O$ values of such rocks to be as low as 2.5‰, much lower than the mantle values (e.g., Gregory and Taylor, 1981; Eiler, 2001; Thirlwall et al., 2006; Wang and Eiler, 2008; Genske et al., 2013). On the other hand, rare-earth elements are generally immobile during hydrothermal alteration so the original mantle-like Sm-Nd and Lu-Hf isotopes of these rocks (Zindler and Hart, 1986) can still be retained after alteration. Thus, the combination of Nd-Hf-O isotopes is a robust tool to evaluate the involvement of the high-T altered grabboic oceanic crust in magma generation.

Oceanic gabbroic rocks commonly have $\varepsilon_{Nd}(t)$ from + 3 to + 15 and $\varepsilon_{Hf}(t)$ from +6 to +18, as represented by MORBs (Chauvel et al., 2008). The $\varepsilon_{Nd}(t)$ values of the uncontaminated magma or least-contaminated magma in

the Emeishan flood province, as represented by picrites in the studied region, are also within this range (e.g., Li et al., 2012). This explains why the involvement of the high-T altered gabbroic oceanic crust in magma generation only decreases $\delta^{18}O$ but not $\varepsilon_{Nd}(t)$ and $\varepsilon_{Hf}(t)$ values (Fig. 8a, b). The involvement of a high-T altered oceanic gabbroic component in magma generation in the mantle is required to explain the zircon Hf-O isotope decoupling in the Taihe deposit (Fig. 8b). Using the end-member compositions of Eiler (2001), Chauvel et al. (2008), and Vervoort et al. (2011), after taking into account ~10 wt.% bulk marble assimilation as indicated by whole-rock Sr-Nd isotopes (Fig. 7), the amount of the high-T altered oceanic gabbroic component in the primary mantle-derived magma of the Taihe deposit is estimated to be ~25 wt.% (Fig. 8b).

It is important to point out that our models shown in Fig. 8b represent only the simplest ones and they are not exclusive of more complicated models. A high-T altered oceanic gabbroic component with low $\delta^{18}O$ may have also involved in the generation of the magmas for the Panzhihua and Hongge deposits but such input was completely masked by relatively high degrees of crustal contamination, or the involvement of other types of recycled oceanic components with relatively high $\delta^{18}O$ values during magma generation. We don't include marble assimilation in our model for the Hongge deposit simply because there is no geological evidence and no requirement for such a process as far as the Sr-Nd-Hf-O isotope data are concerned. Similarly, we don't include contamination with Precambrian metamorphic rock in the model for the Panzhihua and Taihe deposits simply because the isotope data don't require such an interpretation. These different types of contamination could all be involved in the magma differentiation of these deposits, but we focus on the relatively more important one for each deposit.

Incompatible trace element ratios such as LREE/HREE, Th/Nb and La/Ta are commonly used to evaluate crustal contamination and source compositional variation. No systematic variations of these ratios are found between the Hongge, Taihe and Panzhihua intrusions. This is not surprising because these rocks contain variable amounts of Fe-Ti oxides and apatite. The former preferentially retain Nb and Ta but reject the other trace elements whereas the latter retain more LREE than HREE. As a result, the trace element ratios of these rocks do not accurately track those of the trapped magmas. Some of the whole-rock samples from the Taihe intrusion have higher Th/Zr and Rb/Y ratios than those from the Hongge and Panzhihua intrusions (Table Annex I, Hou et al., 2012; Pang et al., 2013; Liao et al., 2015), but the significance of such variations is unclear.

5.4. Implications for ore genesis

The mineralization process of the Panzhihua Fe-Ti-V oxide ore deposits in the Emeishan LIP has been linked to magma-carbonate interaction (Ganino et al., 2013a,b) or olivine fractional crystallization (e.g., Song et al., 2013). The idea that olivine fractional crystallization may induce early Fe-Ti oxide crystallization is based on the assumption that this process will increase Fe^{3+}/Fe^{2+} in the fractionated magma, because olivine only utilizes Fe^{2+} from the magma (Song et al., 2013). The validity of such an assumption for a natural magmatic system is yet to be investigated. In any case, the isotope data from this study cannot be used to evaluate this model, because such a process would have only negligible to no effects on the isotope compositions (Yu et al., 2015). The idea that magma-carbonate interaction is a plausible ore genetic process is based on the concept that addition of CO_2-rich fluids from carbonate country rocks may oxidize the magma significantly to induce over-saturation of Fe-Ti oxides in the contaminated magma (Ganino et al., 2013b). Our Sr-Nd-Hf-O isotope data can be viewed as supporting evidence (Figs. 7 and 8b), although the process proposed by these authors is not bulk assimilation as modelled by us.

Marble assimilation should have significantly increased the $\delta^{18}O$ values of the mantle-derived magma, because the $\delta^{18}O$ values of marbles (7–28‰, Ganino et al., 2013b; Yu et al., 2015) are significantly higher than mantle-derived magma. Marble assimilation by magma would cause elevated $\delta^{18}O$ values for zircon crystallizing from the contaminated magma. The zircon oxygen isotopes of the Panzhihua deposit, and perhaps also the Taihe deposit, are consistent with such an interpretation (Fig. 8b). Finally, we should point out that we are uncertain if the Hf-O isotopes of zircons from a single large sample truly represent the isotope compositions of an ore-bearing zone of a deposit, but such uncertainty can be addressed by analyzing more samples from different localities of a deposit in the future.

6. CONCLUSIONS

Important findings from this study are listed below.

(1) A combination of zircon O-Hf isotopes and whole-rock Sr-Nd isotopes is a more robust tool than is a single isotope system in distinguishing between crustal contamination and mantle source variation for mafic intrusive rocks.
(2) The integrated Sr-Nd-Hf-O isotope data for three coeval magmatic Fe-Ti-V oxide ore deposits in the Emeishan LIP show that these deposits are not linked to a single type of crustal contamination and the same component of the mantle plume.
(3) Marble assimilation is a predominant type of contamination in the Panzhihua and Taihe deposits whereas contamination with Precambrian metamorphic rock is far more important than marble assimilation in the Hongge deposit.
(4) A high-T altered, low $\delta^{18}O$ oceanic gabbroic component in the plume source is required to explain the zircon Hf-O isotope decoupling (mantle-like $\varepsilon_{Hf}(t)$ but lower $\delta^{18}O$ than the mantle) in the Taihe deposit.

(5) Such an unusual component in the plume source is not required to explain the zircon Hf-O isotopes (higher $\delta^{18}O$ than the mantle and lower $\varepsilon_{Hf}(t)$ than the Taihe deposit) of the Panzhihua and Hongge deposits.

Declaration of Competing Interest

The authors declare that they have no known competing financial interests or personal relationships that could have appeared to influence the work reported in this paper.

ACKNOWLEDGMENTS

This study was finally supported by the Second Tibetan Plateau Scientific Expedition and Research Program (STEP) (2019QZKK0704), the Natural Science Foundation of China (41872073, 41472070), the Natural Science Foundation of Gausu Province, China (18JR3RA266), the Fundamental Research Funds for the National Universities of China (lzujbky-2017-77) and Zaozigou Gold Mine, Hezuo, Gansu province. We thank M. Zhang, X. Zhang, Y. Dang, S. Chen, J. Zhang, H. He, J. Li, J. Li and X.H. Li for their assistance in fieldwork, sampling or laboratory analysis. Critical comments from Nicolas Arndt, K-N Pang, and an anonymous reviewer have significantly improved the quality of this paper.

APPENDIX A. SUPPLEMENTARY MATERIAL

Supplementary data to this article can be found online at https://doi.org/10.1016/j.gca.2020.10.006.

REFERENCES

Bai M., Zhong H., Zhu W., Bai Z. and He D. (2013) Platinum-group element geochemical characteristics of the picrites and High-Ti basalts in the Binchuan area, Yunnan Province. *Acta Geol. Sin. (Engl. Ed.)* **87**, 158–840.

Bai Z.-J., Zhong H., Li C., Zhu W.-G., He D.-F. and Qi L. (2014) Contrasting parental magma compositions for the Hongge and Panzhihua magmatic Fe-Ti-V oxide deposits, Emeishan large igneous province, SW China. *Econ. Geol.* **109**, 1763–1785.

Bai Z.-J., Zhong H., Li C., Zhu W.-G. and Xu G.-W. (2012a) Platinum-group elements in the oxide layers of the Hongge mafic-ultramafic intrusion, Emeishan Large Igneous Province, SW China. *Ore Geol. Rev.* **46**, 149–161.

Bai Z.-J., Zhong H., Naldrett A. J., Zhu W.-G. and Xu G.-W. (2012b) Whole-rock and mineral composition constraints on the genesis of the giant Hongge Fe–Ti–V oxide deposit in the Emeishan Large Igneous Province, Southwest China. *Econ. Geol.* **107**, 507–524.

Belousova E. A., Griffin W. L. and O'Reilly S. Y. (2006) Zircon crystal morphology, trace element signatures and Hf isotope composition as a tool for petrogenetic modelling: examples from eastern Australia granitoids. *J. Petrol.* **47**, 329–353.

Blichert-Toft J. (2008) The Hf isotopic composition of zircon reference material 91500. *Chem. Geol.* **253**, 252–257.

Bindeman I. (2008) Oxygen isotopes in mantle and crustal magmas as revealed by single crystal analysis. *Rev. Mineral. Geochem.* **69**, 445–478.

Cao Y., Wang C. Y., Huang F. and Zhang Z. (2019) Iron isotope systematics of the Panzhihua mafic layered intrusion associated with giant Fe-Ti oxide deposit in the Emeishan large igneous province, SW China. *J. Geophys. Res.: Solid Earth* **124**, 358–375.

Chauvel C., Lewin E., Carpentier M., Arndt N. T. and Marini J.-C. (2008) Role of recycled oceanic basalt and sediment in generating the Hf-Nd mantle array. *Nat. Geosci.* **1**, 64–67.

Chen Z.-H. and Xing G.-F. (2016) Geochemical and zircon U-Pb-Hf-O isotopic evidence for a coherent Paleoproterozoic basement beneath the Yangtze Block, South China. *Precambrian Res.* **279**, 81–90.

Chung S.-L. and Jahn B.-M. (1995) Plume-lithosphere interaction in generation of the Emeishan flood basalts at the Permian-Triassic boundary. *Geology* **23**, 889–892.

Corfu F., Hanchar J. M., Hoskin P. W. O. and Kinny P. (2003) Atlas of zircon textures. *Rev. Mineral. Geochem.* **53**, 469–500.

DePaolo D. J. and Wasserburg G. J. (1979) Petrogenetic mixing models and Nd-Sr isotopic patterns. *Geochim. Cosmochim. Acta* **43**, 615–627.

Eiler J. M. (2001) Oxygen isotope variations of basaltic lavas and upper mantle rocks. *Rev. Mineral. Geochem.* **43**, 319–364.

Fan W., Zhang C., Wang Y., Guo F. and Peng T. (2008) Geochronology and geochemistry of Permian basalts in western Guangxi province, southwest China: evidence for plume-lithosphere interaction. *Lithos* **102**, 218–236.

Ganino C., Arndt N. T., Zhou M.-F., Gaillard F. and Chauvel C. (2008) Interaction of magma with sedimentary wall rock and magnetite ore genesis in the Panzhihua mafic intrusion, SW China. *Miner. Deposita* **43**, 677–694.

Ganino C., Arndt N. T., Chauvel C., Jean A. and Athurion C. (2013a) Melting of carbonate wall rocks and formation of the heterogeneous aureole of the Panzhihua intrusion, China. *Geosci. Front.* **4**, 535–546.

Ganino C., Harris C., Arndt N. T., Prevec S. A. and Howarth G. H. (2013b) Assimilation of carbonate country rock by the parent magma of the Panzhihua Fe-Ti-V deposit (SW China): evidence from stable isotopes. *Geosci. Front.* **4**, 547–554.

Gao S., Ling W., Qiu Y., Lian Z., Hartmann G. and Simon K. (1999) Contrasting geochemical and Sm–Nd isotopic compositions of Archean metasediments from the Kongling high-grade terrain of the Yangtze craton: evidence for cratonic evolution and redistribution of REE during crustal anatexis. *Geochim. Cosmochim. Acta* **63**, 2071–2088.

Genske F. S., Beier C., Haase K. M., Turner S. P., Krumm S. and Brandl P. A. (2013) Oxygen isotopes in the Azores islands: Crustal assimilation recorded in olivine. *Geology* **41**, 491–494.

Gregory R. T. and Taylor H. P. (1981) An oxygen isotope profile in a section of Cretaceous oceanic crust, Samail Ophiolite, Oman: Evidence for $\delta^{18}O$ buffering of the oceans by deep (>5 km) seawater-hydrothermal circulation at mid-ocean ridges. *J. Geophys. Res.* **86**, 2737–2755.

Griffin W. L., Wang X., Jackson S. E., Pearson N. J., O'Reilly S. Y., Xu X. S. and Zhou X. M. (2002) Zircon chemistry and magma mixing, SE China: *in-situ* analysis of Hf isotopes, Tonglu and Pingtan igneous complexes. *Lithos* **61**, 237–269.

Hanchar J. M. and Watson E. B. (2003) Zircon saturation thermometry. *Rev. Mineral. Geochem.* **53**, 89–112.

Howarth G. H. and Prevec S. A. (2013) Trace element, PGE, and Sr-Nd isotope geochemistry of the Panzhihua mafic layered intrusion, SW China: Constraints on ore-forming processes and evolution of parent magma at depth in a plumbing-system. *Geochim. Cosmochim. Acta* **120**, 459–478.

Hou T., Zhang Z., Ye X., Encarnacion J. and Reichow M. K. (2011) Noble gas isotopic systematics of Fe-Ti oxide ore-related mafic-ultramafic layered intrusions in the Panxi area, China: the

role of recycled oceanic crust in their petrogenesis. *Geochim. Cosmochim. Acta* **75**, 6727–6741.

Hou T., Zhang Z. C., Encarnacion J. and Santosh M. (2012) Petrogenesis and metallogenesis of the Taihe gabbroic intrusion associated with Fe-Ti oxide ores in the Panxi district, Emeishan Large Igneous Province, southwest China. *Ore Geol. Rev.* **49**, 109–127.

Hu Z., Liu Y., Gao S., Liu W., Yang L., Zhang W., Tong X., Lin L., Zong K., Li M., Chen H., Zhou L. and Yang L. (2012) Improved in situ Hf isotope ratio analysis of zircon using newly designed X skimmer cone and Jet sample cone in combination with the addition of nitrogen by laser ablation multiple collector ICP-MS. *J. Anal. Atom. Spectrom.* **27**, 1391–1399.

Li C., Ripley E. M., Tao Y. and Hu R. (2016) The significance of PGE variations with Sr-Nd isotopes and lithophile elements in the Emeishan flood basalt province from SW China to northern Vietnam. *Lithos* **248–251**, 1–11.

Li C., Tao Y., Qi L. and Ripley E. M. (2012) Controls on PGE fractionation in the Emeishan picrites and basalts: Constraints from integrated lithophile-siderophile elements and Sr-Nd isotopes. *Geochim. Cosmochim. Acta* **90**, 12–32.

Li X. H., Tang G. Q., Gong B., Yang Y. H., Hou K. J., Hu Z. C., Li Q. L., Liu Y. and Li W. X. (2013) Qinghu zircon: a working reference for microbeam analysis of U-Pb age and Hf and O isotopes. *Chin. Sci. Bull.* **58**, 4647–4654.

Li X. H., Li W. X., Li Q. L., Wang X. C., Liu Y. and Yang Y. H. (2010a) Petrogenesis and tectonics significance of the ~850 Ma Gangbian alkaline complex in South China: Evidence from *in situ* zircon U-Pb dating, Hf-O isotopes and whole-rock geochemistry. *Lithos* **114**, 1–15.

Li X. H., Liu Y., Li Q. L., Guo C. H. and Chamberlain K. R. (2009) Precise determination of Phanerozoic zircon Pb/Pb age by multi-collector SIMS without external standardization. *Geochem. Geophys. Geosyst.* **10**, Q04010. https://doi.org/10.1029/2009GC002400.

Li X. H., Long W. G., Li Q. L., Liu Y., Zheng Y. F., Yang Y. H., Chamberlain K. R., Wan D. F., Guo C. H., Wang X. C. and Tao H. (2010b) Penglai zircon megacrysts: A potential new working reference material for micro beam determination of Hf-O isotopes and U-Pb age. *Geostand. Geoanal. Res.* **34**, 117–134.

Liao M., Tao Y., Song X., Li Y. and Xiong F. (2015) Multiple magma evolution and ore-forming processes of the Hongge layered intrusion, SW China: Insights from Sr–Nd isotopes, trace elements and platinum-group elements. *J. Asian Earth Sci.* **113**, 1082–1099.

Luan Y., Song X.-Y., Chen L.-M., Zheng W.-Q., Zhang X.-Q., Yu S.-Y., She Y.-W., Tian X.-L. and Ran Q.-Y. (2014) Key factors controlling the accumulation of the Fe-Ti oxides in the Hongge layered intrusion in the Emeishan large igneous province SW China. *Ore Geol. Rev.* **57**, 518–538.

Ludwig K. R. (2012) *User's Manual for Isoplot 3.75: A Geochronological Toolkit for Microsoft Excel*. Berkeley Geochronol. Center (Spec. Publ. 5).

Morel M. L. A., Nebel O., Nebel-Jacobsen Y. J., Miller J. S. and Vroon P. Z. (2008) Hafnium isotope characterization of the GJ-1 zircon reference materialby solution and laser-ablation MC-ICPMS. *Chem. Geol.* **255**, 231–235.

Pang K. N., Li C., Zhou M.-F. and Ripley E. M. (2008) Abundant Fe-Ti oxide inclusions in olivine from the Panzhihua and Hongge layered intrusions, SW China: evidence for early saturation of Fe-Ti oxides in ferrobasaltic magma. *Contrib. Mineral. Petrol.* **156**, 307–321.

Pang K.-N., Li C., Zhou M.-F. and Ripley E. M. (2009) Mineral compositional constraints on petrogenesis and ore genesis of the Panzhihua layered gabbroic intrusion, SW China. *Lithos* **110**, 199–214.

Pang K.-N., Zhou M.-F., Qi L., Chung S.-L., Chu C.-H. and Lee H.-Y. (2013) Petrology and geochemistry at the Lower zone-Middle zone transition of the Panzhihua intrusion, SW China: Implications for differentiation and oxide ore genesis. *Geosci. Front.* **4**, 517–533.

Panxi Geological Unit, 1984. Mineralization and Exploration Forecasting of V-Ti Magnetite Deposits in the Panzhihua-Xichang Region (in Chinese).

Rudnick R. L. and Gao S. (2003) Composition of the continental crust. *Treat. Geochem.* **3**, 1–64.

Scoates J. S. and Chamberlain K. R. (1995) Baddeleyite (ZrO_2) and zircon ($ZrSiO_4$) from anorthositic rocks of the Laramie anorthosite complex, Wyoming: Petrologic consequences and U-Pb ages. *Am. Mineral.* **80**, 1317–1327.

She Y.-W., Yu S.-Y., Song X.-Y., Chen L.-M., Zheng W.-Q. and Luan Y. (2014) The formation of P-rich Fe-Ti oxide ore layers in the Taihe layered intrusion SW China: implications for magma-plumbing system process. *Ore Geol. Rev.* **57**, 539–559.

Shellnutt J. G., Wang K.-L., Zellmer G. F., Iizuka Y., Jahn B.-M., Pang K.-N., Qi L. and Zhou M.-F. (2011) Three Fe-Ti oxide ore-bearing gabbro-granitoid complexes in the Panxi region of the Permian Emeishan large igneous province, SW China. *Am. J. Sci.* **311**, 773–812.

Song X.-Y., Zhou M.-F., Tao Y. and Xiao J.-F. (2008) Controls on the metal compositions of magmatic sulfide deposits in the Emeishan large igneous province, SW China. *Chem. Geol.* **253**, 38–49.

Song X.-Y., Qi H.-W., Hu R.-Z., Chen L.-M., Yu S.-Y. and Zhang J.-F. (2013) Formation of thick stratiform Fe-Ti oxide layers in layered intrusion and frequent replenishment of fractionated mafic magma: evidence from the Panzhihua intrusion, SW China. *Geochem. Geophys. Geosyst.* **14**, 712–732.

Stacey J. S. and Kramers J. D. (1975) Approximation of terrestrial lead isotope evolution by atwo-stage model. *Earth Planet. Sci. Lett.* **26**, 207–221.

Tanaka T., Togashi S., Kamioka H., Amakawa H., Kagami H., Hamamoto T., Yuhara M., Orihashi Y., Yoneda S., Shimizu H., Kunimaru T., Takahashi K., Yanagi T., Nakano T., Fujimaki H., Shinjo R., Asahara Y., Tanimizu M. and Dragusanu C. (2000) Jndi-1: a neodymium isotopic reference in consistency with Lajolla neodymium. *Chem. Geol.* **168**, 279–281.

Tang Q., Ma Y., Zhang M., Li C., Zhu D. and Tao Y. (2013) The origin of Ni-Cu-PGE sulfide mineralization in the margin of the Zhubu mafic-ultramafic intrusion in the Emeishan large igneous province, SW China. *Econ. Geol.* **108**, 1889–1901.

Tang Q., Li C., Zhang M. and Lin Y. (2015) U-Pb age and Hf isotopes of zircon from basaltic andesite and geochemical fingerprinting of the associated picrites in the Emeishan large igneous province, SW China. *Miner. Petrol.* **109**, 103–114.

Tang Q., Li C., Tao Y., Ripley E. M. and Xiong F. (2017a) Association of Mg-rich olivine with magnetite as a result of brucite marble assimilation by basaltic magma in the Emeishan Large Igneous Province, SW China. *J. Petrol.* **58**, 699–714.

Tang Q., Zhang M., Wang Y., Yao Y., Du L., Chen L. and Li Z. (2017b) The origin of the Zhubu mafic-ultramafic intrusion of the Emeishan large igneous province, SW China: Insights from volatile compositions and C-Hf-Sr-Nd isotopes. *Chem. Geol.* **469**, 47–59.

Tao Y., Li C., Hu R. Z., Ripley E. M., Du A. D. and Zhong H. (2007) Petrogenesis of the Pt-Pd mineralized Jinbaoshan ultramafic intrusion in the Permian Emeishan Large Igneous Province, SW China. *Contrib. Mineral. Petrol.* **153**, 321–337.

Tao Y., Li C., Song X. Y. and Ripley E. M. (2008) Mineralogical, petrological, and geochemical studies of the Limahe mafic-ultramatic intrusion and associated Ni-Cu sulfide ores, SW China. *Miner. Deposita* **43**, 849–872.

Tegner C., Cawthorn R. G. and Kruger F. J. (2006) Cyclicity in the Main and Upper Zones of the Bushveld Complex, South Africa: crystallization from a zoned magma sheet. *J. Petrol.* **47**, 2257–2279.

Thirlwall M. F. (1991) Long-term reproducibility of multicollector Sr and Nd isotope ratio analysis. *Chem. Geol.* **94**(2), 85–104.

Thirlwall M. F., Gee M. A. M., Lowry D., Mattey D., Murton B. J. and Taylor R. N. (2006) Low $\delta^{18}O$ in the Icelandic mantle and its origins: Evidence from Reykjanes Ridge and Icelandic lavas. *Geochim. Cosmochim. Acta* **70**, 993–1019.

Valley J. W. (2003) Oxygen isotopes in zircon. *Rev. Mineral. Geochem.* **53**, 343–385.

Vervoort J. D. and Kemp A. I. S. (2016) Clarifying the zircon Hf isotope record of crust-mantle evolution. *Chem. Geol.* **425**, 65–75.

Vervoort J. D., Plank T. and Prytulak J. (2011) The Hf-Nd isotopic composition of marine sediments. *Geochim. Cosmochim. Acta* **75**, 5903–5926.

Wang Z. and Eiler J. M. (2008) Insights into the origin of low-$\delta^{18}O$ basaltic magmas in Hawaii revealed from *in situ* measurements of oxygen isotope compositions of olivines. *Earth Planet. Sci. Lett.* **269**, 377–387.

Wen X., Guo M. and Ran D. (2008) Status quo, problems and counter measures of Titanium resource utilization in Panzhihua region. *Metal Mine* **386**, 5–29.

Wu F.-Y., Yang Y.-H., Xie L.-W., Yang J.-H. and Xu P. (2006) Hf isotopic compositions of the standard zircons and baddeleyites in U-Pb geochronology. *Chem. Geol.* **234**, 105–126.

Xing C. M., Wang C. Y. and Zhang M. (2012) Volatile and C-H-O isotopic compositions of giant Fe-Ti-V oxide deposits in the Panxi region and their implications for the source of volatiles and the origin of Fe-Ti oxide ores. *Sci. China Earth Sci.* **55**, 1782–1795.

Xiao L., Xu Y. G., Mei H. J., Zheng Y. F., He B. and Pirajno F. (2004) Distinct mantle sources of low-Ti and high-Ti basalts from the western Emeishan large igneous province, SW China: implications for plume- lithosphere interaction. *Earth Planet. Sci. Lett.* **228**, 525–546.

Xu Y., Chung S.-L., Jahn B.-M. and Wu G. (2001) Petrologic and geochemical constraints on the petrogenesis of Permian-Triassic Emeishan flood basalts in southwestern China. *Lithos* **58**, 145–168.

Xu Y.-G., Luo Z.-Y., Huang X.-L., He B., Xiao L., Xie L.-W. and Shi Y.-R. (2008) Zircon U-Pb and Hf isotope constraints on crustal melting associated with the Emeishan mantle plume. *Geochim. Cosmochim. Acta* **72**, 3084–3104.

Yu S.-Y., Song X.-Y., Ripley E. M., Li C., Chen L.-M., She Y.-W. and Luan Y. (2015) Integrated O-Sr-Nd isotope constraints on the evolution of four important Fe-Ti oxide ore-bearing mafic-ultramafic intrusions in the Emeishan large igneous province, SW China. *Chem. Geol.* **401**, 28–42.

Yu S.-Y., Shen N.-P., Song X.-Y., Ripley E. M., Li C. and Chen L.-M. (2017) An integrated chemical and oxygen isotopic study of primitive olivine grains in picrites from the Emeishan Large Igneous Province, SW China: evidence for oxygen isotope heterogeneity in mantle sources. *Geochim. Cosmochim. Acta* **215**, 263–276.

Zhang D., Zhang Z., Mao J., Huang H. and Cheng Z. (2016) Zircon U-Pb ages and Hf-O isotopic signatures of the Wajilitag and Puchang Fe-Ti oxide-bearing intrusive complexes: Constraints on their source characteristics and temporal-spatial evolution of the Tarim large igneous province. *Gondwana Res.* **37**, 71–85.

Zhang Z. C., Mao J. W., Saunders A. D., Ai Y., Li Y. and Zhao L. (2009) Petrogenetic modeling of three mafic-ultramafic layered intrusions in the Emeishan large igneous province, SW China, based on isotopic and bulk chemical constraints. *Lithos* **113**, 369–392.

Zhang Z., Mahoney J. J., Mao J. and Wang F. (2006) Geochemistry of picritic and associated basalt flows of the western Emeishan flood basalt province. *J. Petrol.* **47**, 1997–2019.

Zhang Z., Zhi X., Chen L., Saunders A. D. and Reichow M. K. (2008) Re-Os isotopic compositions of picrites from the Emeishan flood basalt province, China. *Earth Planet. Sci. Lett.* **276**, 30–39.

Zheng Y.-F., Zhang S.-B., Zhao Z.-F., Wu Y.-B., Li X., Li Z. and Wu F.-Y. (2007) Contrasting zircon Hf and O isotopes in the two episodes of Neoproterozoic granitoids in South China: Implications for growth and reworking of continental crust. *Lithos* **96**, 127–150.

Zhong H., Campbell I. H., Zhu W.-G., Allen C. M., Hu R.-Z., Xie L.-W. and He D.-F. (2011a) Timing and source constraints on the relationship between mafic and felsic intrusions in the Emeishan large igneous province. *Geochim. Cosmochim. Acta* **75**, 1374–1395.

Zhong H., Qi L., Hu R.-Z., Zhou M.-F., Gou T.-Z., Zhu W.-G., Liu B.-G. and Chu Z.-Y. (2011b) Rhenium-osmium isotope and platinum-group elements in the Xinjie layered intrusion, SW China: Implications for source mantle composition, mantle evolution, PGE fractionation and mineralization. *Geochim. Cosmochim. Acta* **75**, 1621–1641.

Zhong H., Yao Y., Hu S. F., Zhou X. H., Liu B. G., Sun M., Zhou M. F. and Viljoen M. J. (2003) Trace-element and Sr-Nd isotopic geochemistry of the PGE-bearing Hongge layered intrusion, southwestern China. *Int. Geol. Rev.* **45**, 371–382.

Zhong H., Zhou X. H., Zhou M. F., Sun M. and Liu B. G. (2002) Platinum group element geochemistry of the Hongge Fe-V-Ti deposit in the Pan-Xi area, southwestern China. *Miner. Deposita* **37**, 226–239.

Zhong H. and Zhu W.-G. (2006) Geochronology of layered mafic intrusions from the Pan-Xi area in the Emeishan large igneous province, SW China. *Miner. Deposita* **41**, 599–606.

Zhou M.-F., Robinson P. T., Lesher C. M., Keays R. R., Zhang C.-J. and Malpas J. (2005) Geochemistry, petrogenesis and metallogenesis of the Panzhihua gabbroic layered intrusion and associated Fe-Ti-V oxide deposits, Sichuan Province, SW China. *J. Petrol.* **46**, 2253–2280.

Zhou M.-F., Arndt N. T., Malpas J., Wang C. Y. and Kennedy A. (2008) Two magma series and associated ore deposit types in the Permian Emeishan large igneous province, SW China. *Lithos* **103**, 352–368.

Zhu Y.-H., Yang J.-H., Sun J.-F. and Wang H. (2017) Zircon Hf-O isotope evidence for recycled oceanic and continental crust in the sources of alkaline rocks. *Geology* **45**, 407–410.

Zi J.-W., Fan W.-M., Wang Y. J., Cawood P. A., Peng T.-P., Sun L.-H. and Xu Z.-Q. (2010) U-Pb geochronology and geochemistry of the Dashibao basalts in the Songpan-Ganzi Terrane, SW China, with implications for the age of Emeishan volcanism. *Am. J. Sci.* **310**, 1054–1080.

Zindler A. and Hart S. (1986) Chemical geodynamics. *Annu. Rev. Earth Planet. Sci.* **14**, 493–571.

Associate editor: Weidong Sun